

Genome–lamina interactions are established de novo in the early mouse embryo

Máté Borsos^{1,5}, Sara M. Perricone^{2,5}, Tamás Schauer³, Julien Pontabry¹, Kim L. de Luca², Sandra S. de Vries², Elias R. Ruiz-Morales¹, Maria-Elena Torres-Padilla^{1,4,6*} & Jop Kind^{2,6*}

In mammals, the emergence of totipotency after fertilization involves extensive rearrangements of the spatial positioning of the genome^{1,2}. However, the contribution of spatial genome organization to the regulation of developmental programs is unclear³. Here we generate high-resolution maps of genomic interactions with the nuclear lamina (a filamentous meshwork that lines the inner nuclear membrane) in mouse pre-implantation embryos. We reveal that nuclear organization is not inherited from the maternal germline but is instead established de novo shortly after fertilization. The two parental genomes establish lamina-associated domains (LADs)⁴ with different features that converge after the 8-cell stage. We find that the mechanism of LAD establishment is unrelated to DNA replication. Instead, we show that paternal LAD formation in zygotes is prevented by ectopic expression of *Kdm5b*, which suggests that LAD establishment may be dependent on remodelling of H3K4 methylation. Our data suggest a step-wise assembly model whereby early LAD formation precedes consolidation of topologically associating domains.

We established an experimental procedure to map lamina-associated domains (LADs) using DNA adenine methyltransferase identification (DamID)⁵ with lamin B1, and the untethered DNA adenine methyltransferase (Dam) enzyme as control. Lamin B1 is expressed throughout development and is therefore reliable for profiling LADs (Extended Data Fig. 1a). Temporal control of Dam expression was ensured by using the auxin-inducible degron (AID) system⁶ (Extended Data Fig. 1b, c) and the ^{m6}Atracer⁷ enabled visualization of N⁶-methyladenosine (m⁶A)-modified genome (Fig. 1a, Extended Data Fig. 1b). The experimental conditions did not interfere with embryonic development (Extended Data Fig. 1d, e).

We mapped LADs in fully grown interphase oocytes (GV) arrested at the diplotene stage of prophase, zygotes, 2-cell and 8-cell embryos in populations and single-cell samples. The population replicates and single-cell average profiles displayed high concordance (Extended Data Fig. 1f, g). We also generated LAD profiles in trophoblast and inner-cell-mass (ICM) cells, and in clonal mouse embryonic stem cells. LADs in embryonic stem cells correlate highly with previously published data (Extended Data Fig. 1h) and the similarity in LAD profiles between ICM and embryonic stem cell populations corresponds to the blastocyst origin of embryonic stem cells (Fig. 1b, Extended Data Fig. 1i). Genome–nuclear lamina contacts on autosomes in zygotes, 2-cell, 8-cell and blastocyst-stage embryos revealed broad continuous regions of m⁶A enrichment, characteristic of LADs in somatic cells (Extended Data Fig. 1f), in contrast to those in the Dam-injected embryos (Extended Data Fig. 2a). We conclude that the embryonic genome organizes into LADs in zygotes.

LADs in pre-implantation development display broad domains with a median size of between 1 Mb and 1.9 Mb, and a genomic

coverage of between 42% and 61% (Fig. 1b, c). The 2-cell and 8-cell stages exhibit a larger number of smaller LADs compared with the other stages (Fig. 1b, Extended Data Fig. 3). At the 2-cell and 8-cell stages, 42% of the zygotic LADs reposition to the nuclear interior, but 70% of these zygotic LADs regain association with the nuclear lamina in blastocysts (Fig. 1d). Notably, 86% of LADs in zygotes overlap with LADs in the ICM and share a clear resemblance in associated genomic features (Extended Data Fig. 2b). Zygotic LADs are typified by high AT content, low CpG density and a 67% overlap with previously identified cell-type-invariable constitutive LADs (cLADs)⁸ (Extended Data Fig. 2c). The CpG density and AT content are relatively low in LADs at the 2-cell stage. We postulate that this is the result of a major reorganization of the genome at the 2-cell stage; genomic regions with typical LAD features dislodge from the nuclear lamina, whereas regions with intermediate LAD features associate with the nuclear lamina (Extended Data Fig. 2d). This reorganization in 2-cell embryos involves large, characteristic LAD domains. cLADs make up 77% of the dissociated LADs, further emphasizing the unusual nuclear positioning at the 2-cell stage (Extended Data Fig. 2e). Despite the unusual spatial rearrangements at this stage, repositioning coincides with typical upregulation and downregulation of gene expression in de novo inter-LADs (iLAD) and LADs, respectively (Fig. 1e). LADs that are specific to the 2-cell stage contain genes ($n = 155$) that are mainly expressed in the zygote and at later stages of development, but are generally silent at the mid and late 2-cell stage (Extended Data Fig. 2f). The association between transcriptional changes and spatial repositioning at the 2-cell stage is further illustrated by the markedly stronger repression of minor zygotic genome activation (ZGA) genes in LADs (23% minor ZGA gene density), versus iLADs (15% minor ZGA gene density) (Extended Data Fig. 2d, g). Between the 2-cell and 8-cell stages, differential gene expression also occurs concomitantly with the spatial repositioning of genomic regions (Fig. 1e), and—globally—genes in LADs are transcribed at low levels at the 2-cell and 8-cell stages in comparison to genes in iLADs (Fig. 1f). Examples of transitioning LADs at the 2-cell stage and genes within them are shown in Extended Data Fig. 2h. The less-pronounced differences in gene activity between LADs and iLADs at the 2-cell stage compared with the 8-cell stage may be attributed to a more open chromatin structure at the beginning of development^{9–11} (Extended Data Fig. 2b).

In fully grown oocytes, Dam–lamin B1 profiles appeared indistinguishable from the Dam controls (Fig. 1g, Extended Data Fig. 2i) and lacked LADs typical for all oocyte samples, including single cells. By contrast, reproducible LAD patterns were detected across all zygote samples (Extended Data Fig. 2j). These results suggest that fully grown interphase oocytes are largely devoid of LADs. Together, these data reveal dynamic rearrangements of LADs in accordance with transcription changes, which is suggestive of a gene-regulatory

¹Institute of Epigenetics and Stem Cells (IES), Helmholtz Zentrum München, Munich, Germany. ²Oncode Institute, Hubrecht Institute–KNAW and University Medical Center Utrecht, Utrecht, the Netherlands. ³Bioinformatics Unit, Biomedical Center, Ludwig-Maximilians-University, Planegg, Martinsried, Germany. ⁴Faculty of Biology, Ludwig-Maximilians-Universität, Munich, Germany. ⁵These authors contributed equally: Máté Borsos, Sara M. Perricone. ⁶These authors jointly supervised this work: Maria-Elena Torres-Padilla, Jop Kind. *e-mail: torres-padilla@helmholtz-muenchen.de; j.kind@hubrecht.eu

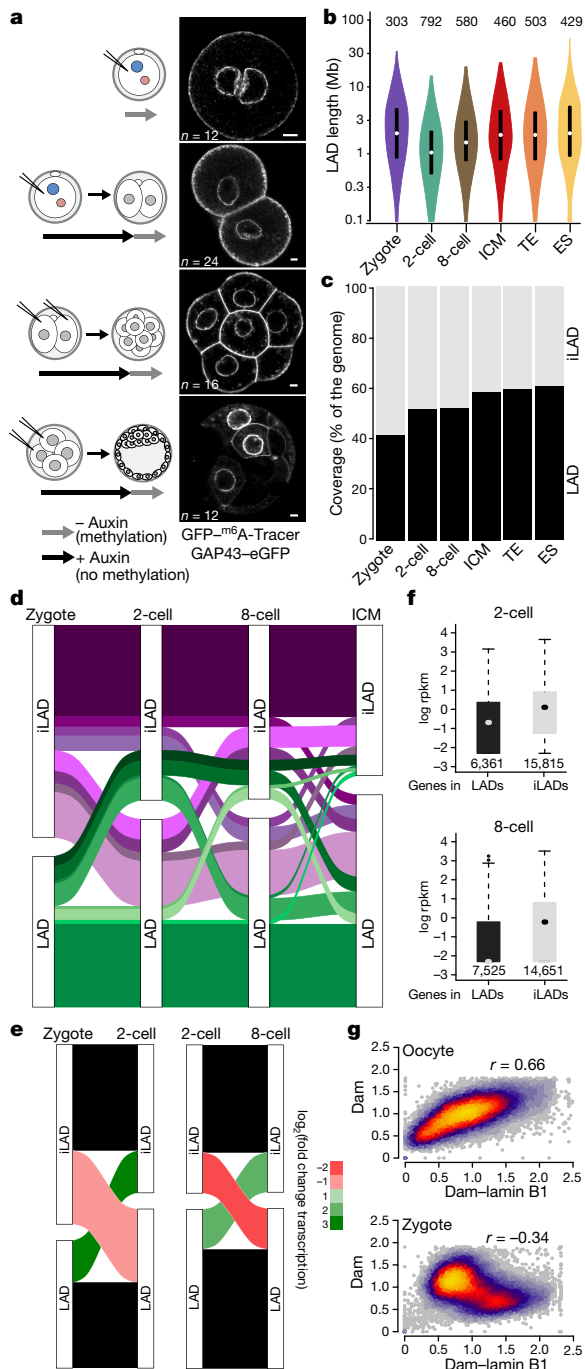


Fig. 1 | LADs establish de novo after fertilization. **a**, Experimental design. LAD methylation upon auxin removal, highlighted by GFP^{-m6A}Tracer. GAP43-eGFP expression marks cell membrane. Scale bar, 5 μ m. Experiments were repeated at least five times. ES, embryonic stem cell. **b**, Distribution of LAD domain length. Violin plots show the 25th and 75th percentiles (black lines), median (circles) and the smallest and largest values within $1.5 \times$ the interquartile range (IQR). n = number of LADs, shown above violin plots. TE, trophoblast. **c**, Genomic LAD coverage. **d**, Alluvial plot showing LAD reorganization during pre-implantation development. **e**, Alluvial plot showing median fold change (\log_2) in expression of genes²⁰ for changing LADs between zygotes, 2-cell and 8-cell stages. **f**, RNA-sequencing (RNA-seq) expression values²⁰ of genes within LADs and iLADs. Box plots show the 25th and 75th percentiles (box), median (circles) and the smallest and largest values within $1.5 \times$ IQR of the hinge (whiskers) and outliers (black circles). n = number of genes, shown below the boxes. **g**, Genome-wide scatter plots (100-kb bins) of Dam and Dam-lamin B1 scores in oocytes and zygotes. n = 3 biologically independent samples.

role of LADs in the early embryo. Furthermore, because typical LADs are undetectable in oocytes, we conclude that in the maternal pronucleus genome–lamina contacts are established de novo after fertilization.

Intra-embryonic heterogeneity in mouse pre-implantation embryos has been linked to cell-fate decisions emerging in the blastocyst¹. To address whether LADs display intra-embryonic heterogeneity, we converted single-cell DamID scores to binary contact frequency maps as previously described¹². Single-cell and population-average LAD profiles display high concordance (Extended Data Fig. 4a). We find that genome–nuclear lamina contacts occur over a wide range of frequencies at all stages (Fig. 2a); nevertheless, overall variability in contact frequency is comparable between individual cells of the three developmental stages (Fig. 2b). Similarly, contact-frequency distributions for zygotes, 2-cell embryos and 8-cell embryos are consistent between variable and constant LADs (Fig. 2a). However, the spatial segmentation in embryonic stem cells appears more consistent, as indicated by the lower coefficient of variation for LADs and iLADs (Fig. 2b). DNA fluorescence in situ hybridization (FISH) coupled with 3D distance measurements on selected LADs and iLADs confirmed the DamID results (Fig. 2c, Extended Data Fig. 4b, c); the mean distance values of DNA FISH showed high positive correlation with the DamID contact frequency scores (Fig. 2d). In addition, DNA FISH confirmed the relocation of selected changing LADs between the 2-cell and 8-cell stages (Extended Data Fig. 4c). Thus, specific and robust nuclear lamina contacts form as early as the zygote and are largely maintained as development progresses.

Next, we used hybrid embryos from mating of F1 (CBA \times C57BL/6J) female mice with CAST/EiJ males to address whether parental differences exist in LADs. Notably, the paternal zygotic genome appears more defined, with broad domains, as opposed to more fragmented patterns with fewer genome–nuclear lamina contacts in the maternal pronucleus (Fig. 2e–g). LAD regions determined by DamID are positioned with similar average distances to the nuclear periphery to those measured by DNA FISH (Extended Data Fig. 4d). However, allele-specific DNA FISH indicates that paternal-specific LADs associate with the nuclear lamina more consistently than do maternal-specific LADs (Extended Data Fig. 4e). Allelic differences persisted until the 8-cell stage, as revealed by *t*-distributed stochastic neighbour embedding (*t*-SNE) (Extended Data Fig. 4f), albeit much less pronounced than in the zygote. DamID on physically separated pronuclei from non-hybrid zygotes confirmed that our observations do not result from a genetic bias derived from different strains (Extended Data Fig. 4f, g). Of note, unlike the paternal zygotic LADs, the maternal LADs are less enriched for typical LAD features and even contain increased DNaseI hypersensitivity (Extended Data Fig. 4h). From the 2-cell stage onwards, LADs showed reduced DNaseI hypersensitivity, which became more pronounced at the 8-cell stage and in embryonic stem cells (Extended Data Fig. 2b). The Pearson correlation between the paternal zygote and 2-cell stage samples is 0.16, which is markedly different from the value of 0.53 for the maternal zygotic versus 2-cell stage (Extended Data Fig. 4i). Jaccard similarity coefficients confirmed these observations (Extended Data Fig. 4j). It therefore appears that the maternal genome–nuclear lamina contacts initiate in the zygote and become reinforced at the 2-cell stage, whereas the paternal genome exhibits clearly defined LADs that are extensively rearranged during the transition from zygote to 2-cell stage.

Whereas LADs are established immediately after fertilization, topologically associating domains (TADs) are largely absent in zygotes and gradually consolidate to form ‘mature’ TADs at late cleavage stages^{13,14}. To address the largely unexplored interdependency between spatial genome organization and the establishment of chromatin topology, we analysed published Hi-C data¹³ and determined insulation scores in the zygote, 2-cell stage, 8-cell stage and ICM at TAD boundaries defined in embryonic stem cells. The insulation scores provide a measure of the overall level of contacts

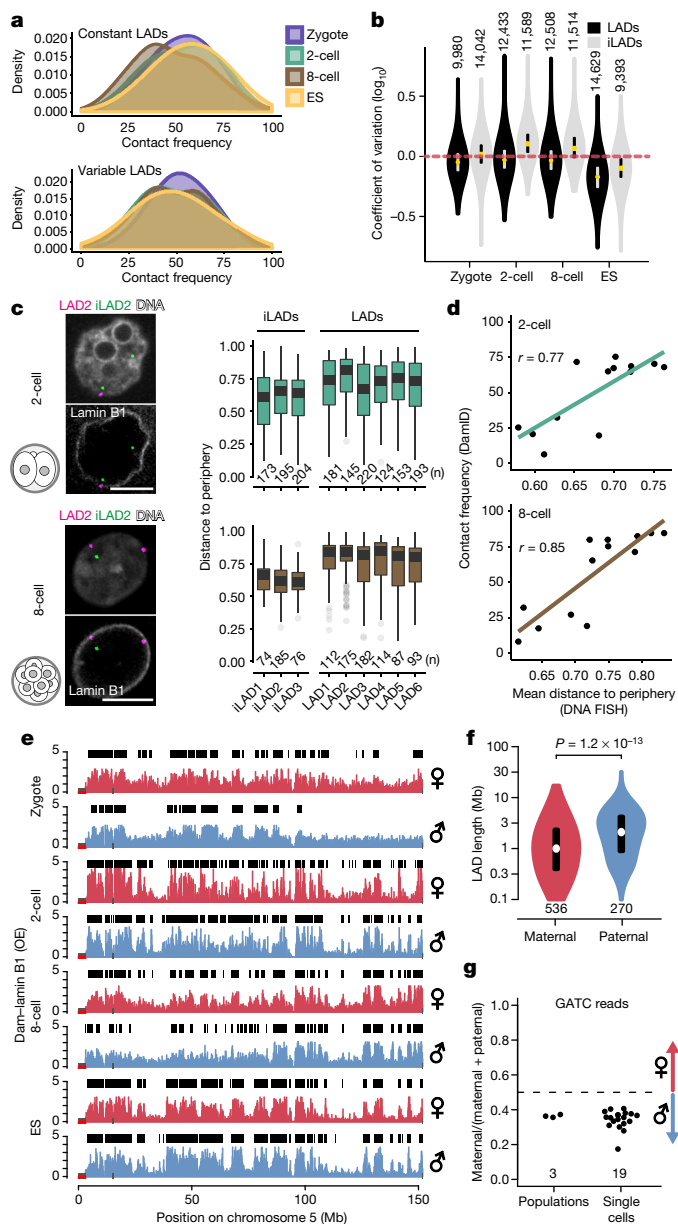


Fig. 2 | Single cells within the same developmental stages show consistent LAD patterning and LADs show parental differences.

a, Density distribution of contact frequencies across stages in constant (top) and variable (bottom) LADs. **b**, Coefficients of variation (\log_{10}) between LADs and iLADs. Violin plots show the 25th and 75th percentiles (black lines), median (circles) and the smallest and largest values within $1.5 \times \text{IQR}$. n = number of 100-kb bins, indicated above violin plot. **c**, Three-dimensional DNA FISH in 2-cell and 8-cell embryos, quantification shows position relative to the nuclear periphery (0, centre; 1, edge). Scale bar, 5 μm . Box plots show the 25th and 75th percentiles (box), median (solid lines) and the smallest and largest values within $1.5 \times \text{IQR}$ of the hinge (whiskers) and outliers (grey circles). n = number of DNA FISH spots from at least three biologically independent samples, shown below the boxes. **d**, Correlation between contact frequency values from DamID and distance measurements from DNA FISH. n = 13 DNA FISH probes (black circles). Pearson's r . **e**, Allelic Dam–lamin B1 profiles. Black boxes represent LAD domains. **f**, Distribution of allelic LAD domain length in zygotes. Two-sided Wilcoxon rank-sum test. Violin plots show the 25th and 75th percentiles (black line), median (circles) and the smallest and largest values within $1.5 \times \text{IQR}$. Number of LADs shown below the violin plot. **g**, Allelic ratio of GATC counts in zygote Dam–lamin B1 samples. n = number of LADs.

that occur over a given genomic region. Because only limited interactions occur between neighbouring TADs, insulation scores are lowest at TAD boundaries¹⁵. As previously shown, TAD boundaries become progressively insulated as development proceeds (Fig. 3a). By contrast, DamID scores projected on per-stage LAD boundaries, reveal that LADs are already clearly defined in zygotes (Fig. 3b), and insulation scores progressively consolidate at the boundaries of zygotic LADs (Fig. 3c). These findings suggest that LADs may precede TAD establishment, and that chromatin scaffolding at the nuclear lamina in the zygote may direct the formation of higher-order chromatin topology throughout early development. Unlike mature TADs, A and B compartments can be observed as early as the zygotic stage, albeit with higher compartment strength in the paternal genome¹³. The majority of LADs overlapped with B compartments in zygotes, 8-cell embryos, ICM and embryonic stem cells (Fig. 3d), consistent with previous findings in embryonic stem cells¹⁶. However, unexpectedly, a substantial proportion of LADs in 2-cell embryos occupies A compartments (39%). This prompted us to investigate whether LADs may help to prime future B compartments. We determined compartment scores stratified for different patterns of LAD dynamics (Extended Data Fig. 5a). Constant iLADs and LADs, respectively, persist as A and B compartments throughout early development (Fig. 3e), which suggests that LAD and compartment formation occur simultaneously for these regions (~50% genome coverage). By contrast, de novo 2-cell-stage LADs that persist as LADs throughout early development (10.8% genome coverage) precede the establishment of B compartments (Fig. 3f). Thus, for certain genomic regions, LADs may help prime the formation of B compartments; however, alternative scenarios exist (Fig. 3f). Interestingly, regions that constitute LADs in zygotes and dislodge from the nuclear lamina at the 2-cell and/or 8-cell stage persist as B compartments throughout early development (Fig. 3g). This is notable, especially because detachment of these regions from the nuclear lamina during the zygote-to-2-cell transition is associated with global transcriptional upregulation of these regions (Fig. 1e). Conversely, nuclear-lamina-associated regions at the 2-cell stage remain as A compartments, yet are associated with global gene repression (Fig. 1e). These data suggest that LADs may be more directive in gene regulation at this stage of development than the not-yet-fully consolidated TADs and compartments.

Finally, we investigated whether LADs, similar to TADs, are affected by blocking replication with aphidicolin¹³. Unlike TADs, zygotic and 2-cell stage LADs remained globally unaffected after aphidicolin treatment, although the patterns appeared less distinctive (Fig. 3h, Extended Data Fig. 5b, c). Similarly to LADs, analysis of published Hi-C data indicated that compartment formation is not affected by aphidicolin (Fig. 3h, Extended Data Fig. 5c). These results indicate that LADs and compartments are established independently of DNA replication. Collectively, our data support a model in which scaffolding of the genome at the nuclear lamina occurs simultaneously with compartment formation but precedes TAD consolidation.

We next investigated the mechanism(s) underlying LAD formation in the zygote. Because LADs are enriched for H3K9me2 and H3K9me3 (hereafter, H3K9me2/me3) in somatic cells^{7,17}, we first tested whether LAD establishment is dependent on H3K9 methylation. We expressed the H3K9 demethylase KDM4D (encoded by *Kdm4d*) in zygotes and performed DamID (Fig. 4a). Lowering global H3K9me2/me3 levels via ectopic expression of *Kdm4d* (Fig. 4b, Extended Data Fig. 6a) had no gross effect on LAD structure (Fig. 4c).

The maternal chromatin contains non-canonical 'broad' H3K4me3 domains, which are established during oocyte growth and persist until ZGA^{18–20}. By contrast, paternal chromatin has significantly lower H3K4me3 levels at fertilization^{21,22}. LADs and iLADs are progressively demarcated by H3K4me3 levels as development proceeds (Fig. 4d); however, only the paternal genome displays clear alternating patterns of H3K4me3 and LAD domains (Extended Data Fig. 6b, c). To address

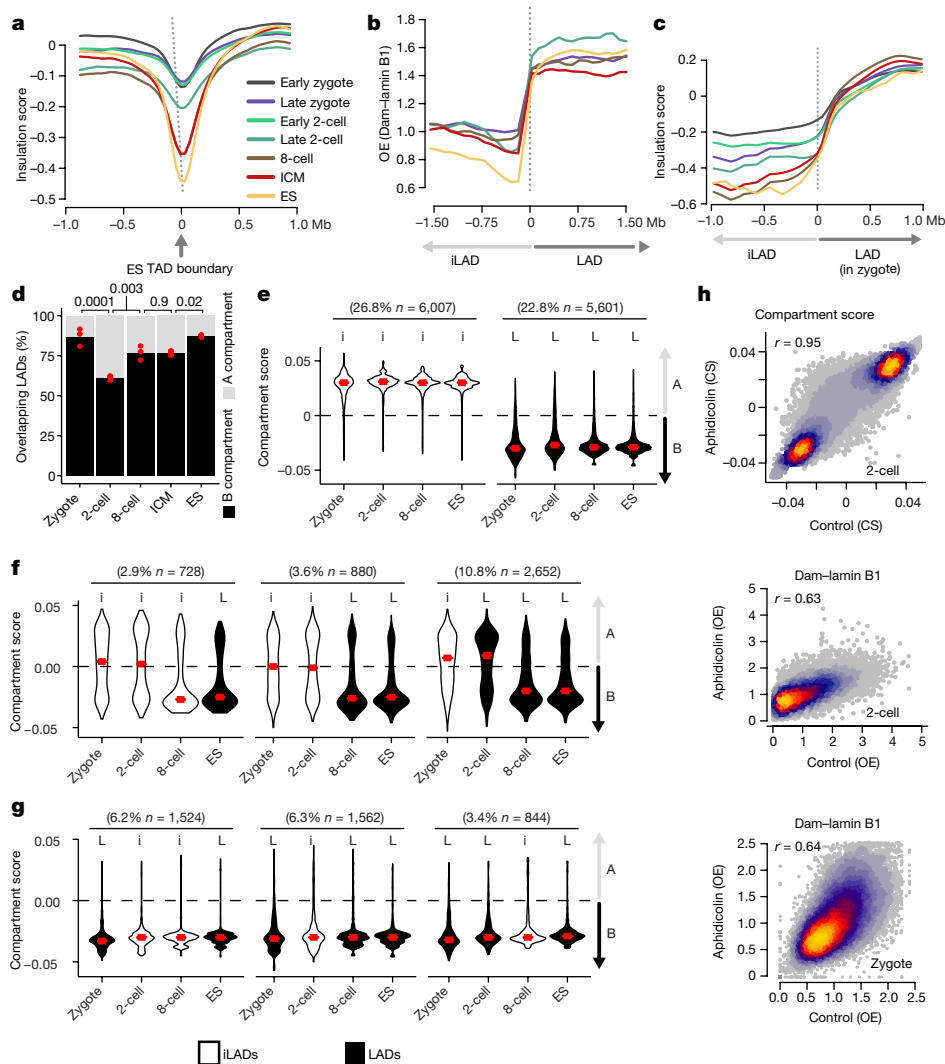


Fig. 3 | Replication unrelated formation of LADs is concordant with A/B compartments and precedes TAD structuring. **a**, Insulation scores from Hi-C data plotted over embryonic stem cell TAD boundaries¹³. **b**, Dam-lamin B1 scores plotted over LAD boundaries. OE, observed/expected (see Methods). **c**, Insulation scores from Hi-C data plotted over zygotic LAD boundaries. **d**, Percentage of LADs overlapping A or B compartments. Data are mean of three biological replicates indicated by red dots. Two-sided post hoc Tukey's test. **e–g**, Violin plots of compartment scores for 100-kb genomic regions with different LAD

dynamics. iLADs and LADs in the indicated stages and embryonic stem cells. The number in parentheses denotes the percentage of the genome covered per category. Violin plots show $1.5 \times$ IQR and median (red lines). Compartment scores are calculated on the basis of three biologically independent samples. n = number of bins. **h**, Genome-wide scatter plots of compartment scores (CS) and DamID scores in control and aphidicolin-treated zygotes and 2-cell embryos. n = 3 biologically independent samples, Spearman's r .

a potential role for H3K4me3 in LAD establishment, we expressed the H3K4me3 demethylase KDM5B (encoded by *Kdm5b*) and performed DamID on physically isolated pronuclei (Fig. 4a). *Kdm5b* expression led to a pronounced reduction of H3K4me3 in both pronuclei compared to controls (Fig. 4e, Extended Data Fig. 6d). Notably, lamin B1 localization, H3K9me2/me3 and global transcriptional activity were unaffected by ectopic expression of *Kdm5b* (Extended Data Fig. 6e–h). Notably, expression of wild-type *Kdm5b*, but not the catalytically inactive mutant, resulted in a near-complete erasure of LAD structure of the paternal genome, with little or no effect on maternal LADs (Fig. 4f, g). The erasure of LAD profiles was consistent across experiments and individual pronuclei analysed (Extended Data Fig. 6i). The same experiment performed in hybrid embryos confirmed these findings (Extended Data Fig. 6j). We conclude that *Kdm5b* is critically involved in de novo establishment of LADs in the paternal pronucleus.

In summary, we show that LADs are established immediately after fertilization without inheritance from the maternal germline. Paternal

inheritance cannot be excluded; however, the de novo acquisition of H3K4me3^{18,21} and the abrogation of LADs upon *Kdm5b* expression in the paternal pronucleus suggests that LADs are formed de novo. The absence of H3K4me3 demarcation of LADs in sperm supports this (Extended Data Fig. 6k, l). De novo H3K4 methylation may support LAD formation or, alternatively, an intact euchromatin compartment may be important for segregating heterochromatin to the nuclear lamina. However, alternative mechanisms that are mediated by KDM5B demethylase activities cannot be formally excluded. Additional investigations are required to further dissect the role of KDM5B and/or H3K4me3 in LAD organization. Our analyses indicate that LAD formation precedes TAD consolidation and may help to prime B compartments for certain genomic regions. It will be important to further dissect the temporal and molecular interdependence of the different levels of nuclear organization. In sum, our work sheds light on the principles behind the establishment of nuclear organization and higher-order chromatin structure during early mammalian development.

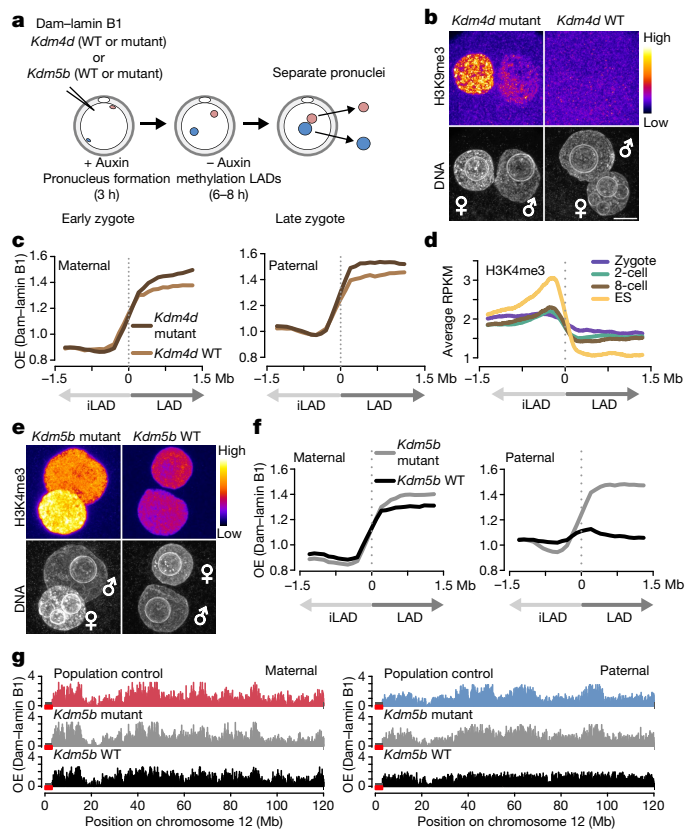


Fig. 4 | Overexpression of *Kdm5b* histone demethylase abrogates paternal LAD establishment in the zygote. **a**, Experimental design. **b**, H3K9me3 immunostaining in zygotes expressing wild-type (WT) or mutant *Kdm4d*. **c**, Average Dam–lamin B1 signal at LAD boundaries in H3K9me3-manipulated embryos. Signal in maternal pronuclei and paternal pronuclei. **d**, Average H3K4me3 signal at LAD boundaries. **e**, H3K4me3 immunostaining in zygotes expressing wild-type and mutant *Kdm5b* mRNA. Scale bars, 10 μ m. **f**, Average Dam–lamin B1 signal at LAD boundaries. **g**, Dam–lamin B1 profiles on maternal and paternal alleles in non-manipulated controls or zygotes expressing wild-type or mutant *Kdm5b*. RPKM, reads per kilobase of transcript per million mapped reads.

Online content

Any methods, additional references, Nature Research reporting summaries, source data, extended data, supplementary information, acknowledgements, peer review information; details of author contributions and competing interests; and statements of data and code availability are available at <https://doi.org/10.1038/s41586-019-1233-0>.

Received: 6 April 2018; Accepted: 12 April 2019;
Published online 22 May 2019.

- Burton, A. & Torres-Padilla, M. E. Chromatin dynamics in the regulation of cell fate allocation during early embryogenesis. *Nat. Rev. Mol. Cell Biol.* **15**, 723–735 (2014).
- Xu, Q. & Xie, W. Epigenome in early mammalian development: inheritance, reprogramming and establishment. *Trends Cell Biol.* **28**, 237–253 (2018).
- Jachowicz, J. W., Santenard, A., Bender, A., Muller, J. & Torres-Padilla, M. E. Heterochromatin establishment at pericentromeres depends on nuclear position. *Genes Dev.* **27**, 2427–2432 (2013).
- van Steensel, B. & Belmont, A. S. Lamina-associated domains: links with chromosome architecture, heterochromatin, and gene repression. *Cell* **169**, 780–791 (2017).
- van Steensel, B., Delrow, J. & Henikoff, S. Chromatin profiling using targeted DNA adenine methyltransferase. *Nat. Genet.* **27**, 304–308 (2001).
- Nishimura, K., Fukagawa, T., Takisawa, H., Kakimoto, T. & Kanemaki, M. An auxin-based degron system for the rapid depletion of proteins in nonplant cells. *Nat. Methods* **6**, 917–922 (2009).
- Kind, J. et al. Single-cell dynamics of genome–nuclear lamina interactions. *Cell* **153**, 178–192 (2013).
- Meuleman, W. et al. Constitutive nuclear lamina–genome interactions are highly conserved and associated with A/T-rich sequence. *Genome Res.* **23**, 270–280 (2013).
- Bošković, A. et al. Higher chromatin mobility supports totipotency and precedes pluripotency in vivo. *Genes Dev.* **15**, 1042–1047 (2014).
- Lu, F. et al. Establishing chromatin regulatory landscape during mouse preimplantation development. *Cell* **165**, 1375–1388 (2016).
- Wu, J. et al. The landscape of accessible chromatin in mammalian preimplantation embryos. *Nature* **534**, 652–657 (2016).
- Kind, J. et al. Genome-wide maps of nuclear lamina interactions in single human cells. *Cell* **163**, 134–147 (2015).
- Du, Z. et al. Allelic reprogramming of 3D chromatin architecture during early mammalian development. *Nature* **547**, 232–235 (2017).
- Ke, Y. et al. 3D chromatin structures of mature gametes and structural reprogramming during mammalian embryogenesis. *Cell* **170**, 367–381 (2017).
- Crane, E. et al. Condensin-driven remodelling of X chromosome topology during dosage compensation. *Nature* **523**, 240–244 (2015).
- Pope, B. D. et al. Topologically associating domains are stable units of replication-timing regulation. *Nature* **515**, 402–405 (2014).
- Wen, B., Wu, H., Shinkai, Y., Irizarry, R. A. & Feinberg, A. P. Large histone H3 lysine 9 dimethylated chromatin blocks distinguish differentiated from embryonic stem cells. *Nat. Genet.* **41**, 246–250 (2009).
- Dahl, J. A. et al. Broad histone H3K4me3 domains in mouse oocytes modulate maternal-to-zygotic transition. *Nature* **537**, 548–552 (2016).
- Liu, X. et al. Distinct features of H3K4me3 and H3K27me3 chromatin domains in pre-implantation embryos. *Nature* **537**, 558–562 (2016).
- Zhang, B. et al. Allelic reprogramming of the histone modification H3K4me3 in early mammalian development. *Nature* **537**, 553–557 (2016).
- Lepikhov, K. & Walter, J. Differential dynamics of histone H3 methylation at positions K4 and K9 in the mouse zygote. *BMC Dev. Biol.* **4**, 12 (2004).
- Torres-Padilla, M. E., Bannister, A. J., Hurd, P. J., Kouzarides, T. & Zernicka-Goetz, M. Dynamic distribution of the replacement histone variant H3.3 in the mouse oocyte and preimplantation embryos. *Int. J. Dev. Biol.* **50**, 455–461 (2006).

Publisher's note: Springer Nature remains neutral with regard to jurisdictional claims in published maps and institutional affiliations.

© The Author(s), under exclusive licence to Springer Nature Limited 2019

METHODS

Oocyte and embryo collection and manipulation. Experiments with animals were carried out according to valid legislation in France and under the authorization of the Cometh Institute of Genetics, Molecular and Cellular Biology ethical committee and in compliance with the local government (Government of Upper Bavaria). Pre-implantation embryos were collected from 5–8-week-old F1 (CBA × C57BL/6J) female mice mated with CAST/Eij males for hybrid crosses and with F1 males for non-hybrid crosses. Ovulation was induced by injecting 10 IU pregnant mare serum gonadotropin (PMSG) (IDT Biologika) and then human chorionic gonadotropin (hCG) (MSD Animal Health) 46–48 h later. GV oocytes were collected 44–48 h after PMSG injection. Reciprocal crosses (CAST/Eij females mated with F1 males) were performed without inducing ovulation. Oocytes were cultured in IBMX containing M16, whereas embryos were cultured in KSOM drops under paraffin oil (Sigma). The sample size was not chosen. In each experiment, embryos from 4–8 female mice were pooled and randomly allocated to experimental groups. No blinding was done, because no manual assessment of images or experiments was performed. For DamID, an mRNA mixture containing 250 ng/μl *Tir1*, 50 ng/μl membrane-eGFP and embryonic stage-dependent concentrations of AID–Dam–lamin B1 or AID–Dam were injected into the cytoplasm of oocytes and embryos. Fifty nanograms per microlitre AID–Dam–lamin B1 mRNA injected from zygote to 2-cell stage—fivefold-higher mRNA concentration than otherwise used to map LADs at the 2-cell stage. To methylate LADs only at the stages of interest, we washed the embryos into auxin-free medium for 6–8 h at the late-S and G2 phases of the cell cycle. Oocytes (48 h post PMSG) and zygotes (21 h post hCG) were isolated and injected with 5 ng/μl AID–Dam–lamin B1 or 20 ng/μl AID–Dam and kept in auxin-free KSOM for 6–8 h to methylate LADs or accessible regions, respectively. We performed additional DamID experiments in oocytes using 20 and 50 ng/μl of AID–Dam–lamin B1 mRNA, and obtained similar results to those obtained using only 5 ng/μl (GSE112551). For DamID at 2-cell stage late zygotes (27–28 h post hCG) were isolated and injected with 10 ng/μl AID–Dam–lamin B1 or 40 ng/μl AID–Dam in auxin (500 μM)-containing medium. Auxin was removed at 2-cell stage for 6–8 h (from 42 to 48–50 h post hCG). For DamID at 8-cell stage, late 2-cell embryos (46–48 h post hCG) were isolated and injected with 20 ng/μl AID–Dam–lamin B1 or 40 ng/μl AID–Dam in auxin-containing medium. Auxin was removed at the 8-cell stage for 6–8 h (from 66 to 72–74 h post hCG). Afterwards, the zona pellucida was removed by treatment with 0.5% pronase in M2 at 37°C and the polar bodies were mechanically separated from the embryos and discarded. Pools of either 20 blastomeres or single blastomeres were placed into 2 μl DamID buffer (10 mM TRIS acetate pH 7.5, 10 mM magnesium acetate, 50 mM potassium acetate) and stored at –80°C until downstream processing. For the ICM and trophectoderm samples, 4-cell embryos were injected with 100 ng/μl AID–Dam–lamin B1 or Dam mRNA at 60–62 h post hCG injection. Indole-3-acetic acid (IAA) was washed out at 90 h post hCG when blastocysts started to cavitate. Embryos were treated with pronase at 96 h and incubated in Fluorospheres (F8811 – Sigma) to mark trophectoderm cells for 2 min. Residual Fluorospheres were washed away and embryos were kept in calcium-free M2 medium for 25 min followed by mechanical disaggregation. Fluorosphere-positive trophectoderm cells were separated from negative ICM cells under a fluorescent microscope and placed into DamID buffer.

For DamID in embryos expressing *Kdm5b* or *Kdm4d*, early zygotes from non-hybrid crosses (18 h post hCG) were injected with 2 μg/μl wild-type or mutant *Kdm5b* or 1.8 μg/μl wild-type or mutant *Kdm4d*, and 5 ng/μl AID–Dam–lamin B1, and 250 ng/μl TIR1 and 50 ng/μl membrane-eGFP coding mRNA. Zygotes were kept in auxin-containing KSOM for 3 h to prevent adenine methylation during pronucleus formation. At 21 h post hCG auxin was removed for 6–8 h to allow methylation. To separate pronuclei, the PN5 zygotes were transferred to M2 medium containing 10 μg/ml cytochalasin B (Sigma-Aldrich). The zona pellucida was cut with a Piezo-driven micromanipulator and one of the pronuclei was isolated into M2 drops. The pronuclei were distinguished based on their size and their relative position to the second polar body. The remaining embryos containing a single pronucleus were treated with pronase to remove the zona pellucida and the polar bodies were discarded. The karyoplasts and the single pronuclei containing embryos were frozen in DamID buffer as above. For DamID in replication inhibited 2-cell embryos, late zygotes (26–28 h post hCG) from hybrid crosses (CBA × C57BL/6J females mated with CAST/Eij males) were injected with 10 ng/μl AID–Dam–lamin B1, 250 ng/μl TIR1 and 50 ng/μl membrane-eGFP coding mRNA and kept in auxin-containing medium to prevent Dam activity in the zygote. Embryos were washed into aphidicolin (3 μg/ml)-containing medium when reaching the first metaphase. Auxin was removed from 42 to 48–50 h post hCG to allow methylation of LADs in the late 2-cell stage.

Plasmid construction and mRNA production. The cDNA encoding wild-type *Kdm5b* was obtained from Addgene (86398)²⁰. To generate a catalytically inactive version of *Kdm5b* the H499A mutation was introduced by site-directed mutagenesis. The in vitro transcription plasmids containing the wild-type and mutant

Kdm4d were obtained from Addgene (61553, 61554)²³. mRNA was transcribed in vitro with T7 or T3 mMESSAGE mMACHINE kits (Ambion) and purified by LiCl precipitation. All plasmids generated in this study are available at Addgene under ‘Torres-Padilla lab plasmids’.

Immunofluorescence. Embryos were treated with 0.5% pronase in M2 to remove zona pellucida at 37°C, washed in PBS and fixed in 4% PFA for 15 min at room temperature. After permeabilizing in 0.5% Triton-X 100 in PBS for 20 min, embryos were kept in blocking buffer (3% BSA in PBS) from one hour to overnight. Embryos were incubated overnight in primary antibody mixes (Supplementary Table 1) diluted in blocking buffer, washed three times in PBS and stained with secondary antibodies conjugated with (Alexa Fluor 488, Alexa Fluor 568, Alexa Fluor 594 or Alexa Fluor 647) in blocking buffer for one hour. After washing three times in PBS, embryos were mounted in Vectashield containing DAPI. Lamin B1 is also known to be expressed in oocytes and blastocysts, as assessed by western blot²⁴. For visualizing global transcription, zygotes were pulsed with 50 μM EU for one hour (26–27 h post hCG) and visualized with the Click-iT RNA Alexa Fluor 594 Imaging Kit (Thermo Fisher) according to the manufacturer’s instructions. For visualizing global DNA replication, zygotes or 2-cell embryos were pulsed with 10 μM EdU and visualized with the Click-iT EdU Alexa Fluor 594 Imaging Kit according to the manufacturer’s instructions (Thermo Fisher).

DNA FISH. DNA FISH was performed as previously described, using a protocol that preserves 3D information²⁵. BACs were obtained from BACPAC or RIKEN DNABank (Supplementary Table 1) and purified with NucleoBond Xtra Midi Plus kit (Macherey-Nagel). BACs were nick-translated with 5-TAMRA, Atto594 and Atto647N conjugated dUTPs according to the manufacturer’s instructions (Roche). To combine nuclear envelope staining with DNA FISH, immunostaining was performed with mAb414 (1:1,000; Abcam) as described above, followed by postfixation in 2% PFA for 10 min. Next, embryos were washed in 0.5% Triton-X 100 for 10 min and treated with HCl solution (0.1N HCl, 0.5 Triton-X 100 and 1 mg/ml PVP in water) for 90 s, washed into prehybridization buffer (50% formamide, 1 mg/ml PVP, 0.05% TritonX, 0.5 mg/ml BSA) and incubated at 37°C for one hour. Embryos were transferred into drops of 0.2 μl hybridization buffer (prehybridization buffer containing 1 μg/μl mouse Cot-1 DNA) under mineral oil, denatured at 80°C for 10 min and incubated at 37°C for one hour. Embryos were transferred into drops of 0.2 μl hybridization buffer containing a mixture of three probes, each at 5 ng/μl which were previously denatured at 80°C for 10 min under oil. After overnight hybridization at 37°C, embryos were washed twice in 2× SSC, 0. Triton-X 100, 1 mg/ml PVP at room temperature followed by washing three times 10 min in 2× SSC, 0. Triton-X 100, 1 mg/ml PVP at 55°C and mounted in Vectashield containing DAPI on slides with spacers (Grace Bio-Labs SecureSeal) to preserve 3D structure.

Imaging and analysis. Microscopy images were acquired on a Leica SP8 confocal microscope equipped with a Plan Apochromat 63×/1.4 oil objective at 1.5-μm *z* steps for immunofluorescence and at 0.3-μm *z* steps for DNA FISH. H3K4me3, lamin B1 and EU intensity was quantified in the nuclei defined by creating masks on the DAPI staining using a custom made Icy protocol (<http://icy.bioimaginganalysis.org/>). DNA FISH spots were identified and their distance was measured relative to the DAPI mask periphery using another custom made Icy protocol. The centre of the DAPI mask was defined as 0 and the location of FISH spots along the unit vector from the centre (0) to the periphery (1) was determined. Immunofluorescence signal intensities of all experimental groups were normalized to the median of the control group’s (KDM5B mutant) intensity separately for each biological replicate. The differences in signal intensity and FISH spot distance were subjected to Wilcoxon signed-rank test between groups or stages of development. For each stage, between 71 and 220 FISH spots were analysed.

Hi-C data analysis. Data for untreated embryos were used from GSE82185, for the aphidicolin-treated and their control 2-cell embryos from PRJCA000241. Raw files from all biological replicates were pooled and analysed with HiC-Pro (version 2.10.0)²⁶ as described in ref.¹⁵ but aligning to the mm10 mouse reference genome. Compartments were called using the HiTC package²⁶. Iterative correction and eigenvalue decomposition-normalized 100-kb interaction matrices were binned with a bin size of 500 kb and a step size of 100 kb. Observed/expected matrices were used to generate correlation matrices and perform principal component analysis. A and B compartments were defined by the first principal component and gene density. TADs and insulation scores were calculated as described⁴.

Cell culture. F1 hybrid 129/Sv:Cast/Eij mouse embryonic stem cells²⁶ were cultured at 37°C, 5% CO₂ on primary mouse embryonic fibroblasts, in Glasgow’s minimum essential medium (G-MEM; Gibco cat. no. 21710025) supplemented with 10% fetal bovine serum (FBS; Gibco cat. no. F7524), 1% penicillin–streptomycin (Gibco cat. no. 15140122), 1% GlutaMAX (Gibco cat. no. 35050038), 1% non-essential amino acids (Gibco cat. no. 11140035), 1% sodium pyruvate (Gibco cat. no. 11360039), 143 μM β-mercaptoethanol (Sigma cat. no. M6250) and 1:1,000 human leukaemia inhibitor factor (LIF; in-house production). F1 hybrid 129/Sv:Cast/Eij mouse embryonic stem cells were not authenticated; they tested negative for mycoplasma.

Generating cell lines. Stable clonal Dam and Dam–lamin B1 lines were created by transfection of EF1 α -Tir1-*neo* with hPGK-AID-Dam–lamin B1 or hPGK-AID-Dam plasmids in a ratio of 1:5 plasmids with Effectene (Qiagen cat. no. 301427). Clones were selected with 250 μ g/ml G418 (Thermo Fisher cat. no. 10131035) and selection of the clones was based on methylation levels as determined by DpnII-qPCR assays as previously described⁷. To reduce the background methylation levels in the presence of 1.0 mM IAA (Sigma cat. no. 15148), we transduced the selected clones of both AID-Dam–lamin B1 and Dam with extra hPGK-Tir1-puro followed by selection with 0.8 μ g/ml puromycin (Sigma cat. no. P8833-10mg). Positive clones were screened for IAA induction by DpnII-qPCR assays and DamID PCR products⁷.

DamID induction and collection. Expression of AID–Dam and AID–Dam–lamin B1 was suppressed by culturing the cells in the presence of 1.0 mM IAA for 48 h. DamID was induced by IAA washout 12 h before collection. Twelve hours after IAA washout, cells were collected in G-MEM supplemented with 10% FBS and 1% penicillin–streptomycin and stained with 10 μ g/ml Hoechst 34580 (Sigma cat. no. 911004450) for 45 min at 37°C. Single-cell or 20-cell populations were sorted in 96-well plates at G2/M phase of the cell cycle based on the DNA content histogram. **Single-cell DamID.** We sequenced three independent population samples (of 15, 20 or 24 cells) for zygotes, 2-cell and 8-cell stage, respectively, and a total of 327 single cells for all stages. Single cells or populations of cells were manually sorted in 8-well PCR strips in 2 μ l of DamID buffer (10 mM TRIS acetate pH 7.5 (Sigma cat. no. T1258); 10 mM magnesium acetate (Sigma cat. no. 63052); 50 mM potassium acetate (Sigma cat. no. 95843); 2.01% Tween-20 (Sigma cat. no. P2287). One microlitre lysis buffer with proteinase K (10 mM TRIS acetate pH 7.5 (Sigma cat. no. T1258); 10 mM magnesium acetate (Sigma cat. no. 63052); 50 mM potassium acetate (Sigma cat. no. 95843); 2.01% Tween-20 (Sigma cat. no. P2287); 2.01% Igepal (Sigma cat. no. I8896) and 2.01 mg/ml proteinase K (Roche cat. no. 03115828001)) was added to the samples, followed by proteinase K digestion at 42°C for 12 h in a thermoblock with heated lid. Proteinase K was inactivated by heating the samples for 20 min at 80°C. In the following steps, reagents were added with an Eppendorf Multipipette Plus mounted with a 0.1-ml Combitip (Eppendorf cat. no. 0030089405). The surface of the reaction volume was never touched by the pipette tip. Genomic DNA (gDNA) was digested for 8 h by the addition of 7 μ l of DpnI reaction mix (0.1 μ l DpnI (10 U/ μ l, New England Biolabs cat. no. R0176L); 0.7 μ l 10 \times One-Phor-all-buffer plus (100 mM Tris acetate pH7.5; 100 mM magnesium acetate; 500 mM potassium acetate) and 6.2 μ l nuclease-free H₂O) and incubation at 37°C in a PCR block, followed by heat inactivation at 80°C for 20 min. Adaptor ligation was performed by the addition of 10 μ l ligation mix (2 μ l 2 \times T4 ligation buffer; 0.5 μ l T4 ligase (5 U/ μ l, Roche cat. no. 10799009001); 0.05 μ l 50 μ M double-stranded DamID adaptor²⁷ and 7.3 μ l nuclease-free H₂O) and incubation in a PCR block at 16°C overnight. Heat inactivation at 65°C for 10 min the next day was followed by PCR amplification by the addition of 30 μ l PCR mix (10 μ l 5 \times MyTaq Red reaction buffer (Bioline cat. no. 25043), 1.25 μ l PCR barcoded primer (50 μ M) NNNNNNBARCODGTGGTCGCGCCGAGGATC (Supplementary Table 2), 0.5 μ l MyTaq DNA polymerase (Bioline cat. no. 25043) and 18.25 μ l nuclease-free H₂O). The PCR primer carries 6 random nucleotides at the 5' end to meet the Illumina software requirements of generating reads with diverse starting sequences and a 6-nucleotide sample barcode (Supplementary Table 2). The thermal cycling scheme is as follows: (1) 72°C for 10 min; (2) 94°C for 1 min, 65°C for 5 min and 72°C for 15 min; (3) 94°C for 1 min, 65°C for 1 min and 72°C for 10 min (4 times); (4) 94°C for 1 min, 65°C for 1 min and 72°C for 2 min (29 times, or 27 times for the population samples).

Of the resulting PCR product, 8 μ l was used for standard 1% agarose gel electrophoresis for analytical purpose and estimation of DNA concentration. All samples were pooled and prepared for Illumina sequencing.

Single-cell DamID Illumina library preparation and sequencing. Of 300 ng purified PCR product the 3' or 5' overhanging ends were blunted in a 50- μ l reaction following the manufacturer's instructions (End-It DNA End-Repair Kit, Epicentre cat. no. ER81050). The blunted DNA samples were again purified using the PCR purification columns of Qiagen and eluted with 26 μ l nuclease-free H₂O. Next, a 3' adenine was added by incubation for 30 min at 37°C in a 50- μ l reaction mix (1 \times New England Biolabs restriction buffer 2, 200 μ M dATP (Roche cat. no. 11051440001) and 25 units of Klenow 3' \rightarrow 5' *exo*- (New England Biolabs cat. no. M0212M). After heat inactivation at 75°C for 20 min, the DNA was purified with Agencourt AMPure XP beads (Beckman Coulter cat. no. A63881). A 1.8 \times volume of beads over DNA sample was used, manufacturer's instructions were followed and the DNA was eluted with 20 μ l nuclease-free H₂O. To the purified DNA, the Illumina indexed Y-shaped adapters (TruSeq Nano DNA LT Library Prep Kit cat. no. FC-121-4402) were then ligated for 2 hours at room temperature in a 40 μ l reaction mix (4 μ l 10 \times T4 ligation buffer, 0.5 μ l T4 ligase (5 U/ μ l) Roche cat. no. 10799009001, 2.5 μ l Illumina adaptor, with nuclease-free H₂O added to 40 μ l final volume). Next, the T4 ligase reaction was heat-inactivated at 65°C for 10 min followed by 2 \times DNA purification with 1.8 \times volume followed by 1.2 \times volume

AMPure beads as described for the previous step. For the addition of the Illumina index primers, a PCR reaction was performed with the DNA from the previous step in a 20 μ l MyTaq red DNA polymerase PCR reaction mixture (10 μ l 2 \times MyTaq reaction mixture (Bioline cat. no. BIO21110), 1 μ l 2.5 μ M Illumina oligo mix, nuclease-free H₂O to a final volume of 20 μ l). The DNA was amplified for 6–8 PCR amplification cycles (94°C 1 min; 94°C 30 s, 58°C 30 s and 72°C for 30 s for nine cycles and 72°C for 2 min) after which 5 μ l of each sample was analysed by agarose gel electrophoresis. For Illumina multiplex sequencing, typically 4 to 10 separate libraries—each with 20–50 single cells—were mixed in approximate equimolar ratios as judged from the agarose gel image. The pooled sample was subjected to a Qiagen PCR column purification and subsequent AMPure bead purification with 1.6 \times volume of beads over DNA sample before it was used for sequencing.

Processing of single-cell DamID sequencing reads. Base calling and filtering were performed using standard software of the Illumina HiSeq 2500. The total number of raw and final GATC reads are shown in Supplementary Table 3. Sequenced 151-bp reads were parsed to obtain the gDNA for downstream analysis. When present, the first 6 random bases were discarded; subsequently, the reads were demultiplexed and the 15 bp of adaptor trimmed using custom scripts and cutadapt²⁸. The pre-processed reads were then mapped to the mm10 (or alternative genome assemblies) using bwa aln v.0.7.12²⁹ with default parameters. Reads aligning to the genome with quality score below 25 were discarded. Note that we applied a stringent threshold for the quality of the DamID datasets throughout all of the experiments, which we set at minimum 30,000 unique reads. Therefore, all the libraries that did not reach this level of quality were discarded from the analysis. The computation of OE value per bin was carried out as described¹². In brief, reads that precisely flanked an annotated GATC site were associated with GATC fragments and kept for downstream analysis. To compare population samples to single-cell samples, multiple reads aligning to the same position were counted as one and subsequently aggregated in genomic segments of 100 kb to determine the experimentally observed value. This was then divided by the expected value per 100-kb bin. The expected value was generated by *in silico*-determining potential DamID sequencing reads of the same length as the experimental data (~131 bp), aligning them to the mm10 genome assembly and selecting them based on the same filtering applied to the experimental data and aligned to GATC-fragments (see above). The final OE value per 100-kb bins was computed by dividing the ratio of the two counts (observed and expected) by the total number of observed reads per bin. LAD domain calling was performed on the average population replicates for each stage in (parental or non-allelic) OE values calculated using a two-state hidden Markov model (HMM)³⁰, which allows the classification of each 100-kb segment as LAD or iLADs. The computation of contact frequency scores was carried out as described in ref. ¹², by binarization of the OE values and subsequent summation of the contact frequency score across the single-cell samples per 100-kb bin.

Identification of parental-specific reads. For hybrid samples C57BL/6 \times CAST/Eij or 129/Sv \times CAST/Eij, CAST/Eij and 129/Sv genomes were *de novo*-compiled by nucleotide substitution of strain specific single nucleotide polymorphisms (SNPs) using the SNPsplit_genome_preparation tool (v.0.3.0/) (<http://www.bioinformatics.babraham.ac.uk/projects/SNPsplit/>) in the original mm10 genome assembly. The database of annotated SNPs between different mouse strains was obtained from ftp://ftp-mouse.sanger.ac.uk/current_snps/strain_vcfs/. The reads were separately aligned to the parental (mm10 or hybrid) genomes using the above described parameters. The edit distance of the alignments of pre-filtered reads (quality score \geq 25) was compared to the two genomes. The reads aligning with the lowest edit distance were assigned to the appropriate parental genome. The reads aligning with equal edit distance between the parental genomes were not assigned to the parental genomes but were kept for 'non-allelic' profiles.

Comparative genomics to published datasets. Low-input chromatin immunoprecipitation (ChIP) data for H3K4me3 and DNA-hypersensitivity data were obtained from Gene Expression Omnibus (GEO) accession numbers GSE71434 and GSE76642, respectively. Alignment was carried out as described for the DamID sequencing reads. Picard tools (v.1.130) (<http://picard.sourceforge.net>) was used to remove PCR duplicates. Additionally, as the H3K4me3 arises from a mouse mixed genetic background C57BL/6N \times PWK, the assignment of reads belonging to parental genomes was carried out as described for the DamID libraries. Normalization in reads per million (RPM) was then carried out in fixed genomic windows of 5 kb or 100 kb to allow direct comparison with DamID data. Gene expression data were obtained from GEO accession GSE71434. The samples were aligned to the mm10 genome assembly using hisat2 (v.2.0.3-beta³¹) with default parameters. Reads mapping with quality score lower than 200 were discarded. htseq-count (v.0.6.0)³² was then used to assign the mapped reads to a transcriptional model file (gencode.vM9.annotation.gtf) obtained from (<https://www.gencodegenes.org>). Only genes annotated in the refFlat (<http://hgdownload.soe.ucsc.edu/goldenPath/mm10/database/>) database were considered for downstream analysis. The RPKM values were calculated for each gene by normalizing the total

number of mapped reads per gene by the gene length in kb and sample size. A gene transcription start site was considered to be located within a LAD when the region surrounding its transcription site (± 250 bp) was located within a LAD. edgeR³³ was used to perform differential expression analysis between consecutive stages. A given gene was considered significantly changing if the associated false-discovery-rate (FDR)-corrected P values is ≤ 0.01 . Maternal-specific genes³⁴ were depleted from this analysis. For the expression of minor ZGA genes, the datasets identified in ref.³⁴ was used (clusters 5–8). Minor ZGA genes undergo downregulation by the 4-cell stage. The minor ZGA gene dataset was omitted for the differential expression analysis to compare the 2-cell stage and 8-cell stages in Fig. 1g. For the heat map in Extended Fig. 2e, we defined the expression of the genes inside the LADs using the single-cell RNA-seq data in ref.³⁵. The counts were quantified using kallisto software (v.0.44.0)³⁶. An RPKM normalization was applied to the raw counts using the R package edgeR; only those genes with counts > 1 RPKM on average were considered as expressed. We calculated the mean expression of each gene per developmental stage and their z -scores were computed to visualize the relative gene expression between the stages, these values were plotted as a heat map using the R package Pheatmap. For the comparison with previously obtained DamID data on LADs in embryonic stem cells³⁷, the processed data were obtained from GEO accession GSM426758 in the form of \log_2 Dam–lamin B1 scores. To directly compare this dataset to the data generated in our study, average \log_2 Dam–lamin B1 scores were calculated for fixed genomic windows of 100 kb. HMM was then applied to call LADs in the different cell types obtained from GSM426758. Regions (100 kb) were finally defined as ‘cLADs’ if they were classified as LADs in each of the individual cell types described in¹². For Fig. 1g, genes were considered significantly changing if the associated FDR-corrected $P \leq 0.01$. edgeR³³ was used to perform differential expression analysis between consecutive stages. Only the fold change (expressed in \log_2) of significantly differentially expressed genes between zygote and 2-cell, and 2-cell and 8-cell stages were included in the analysis. Figure 1g displays the median \log_2 fold change for changing LADs between zygote and 2-cell stage and 2-cell and 8-cell stage. Maternally specific genes as defined in ref.³⁶ were removed from this analysis to prevent confounding effects owing to mRNA degradation. For similar reasons, the minor ZGA gene dataset based on ref.³⁶ (clusters 5–8) was omitted for the differential expression analysis between the 2-cell and 8-cell stages. This was decided because these mRNAs gradually decrease from the 2-cell to 8-cell transition but are still relatively highly abundant at the 2-cell stage compared to the 8-cell stage. Because of the unequal abundance of minor ZGA mRNA, gene expression appears artificially inflated at the 2-cell stage. As a result, gene expression at the 8-cell stage would appear downregulated overall compared to the 2-cell stage if not corrected for minor ZGA genes.

Statistical testing. No statistical methods were used to predetermine sample size. The experiments were not randomized. The investigators were not blinded to allocation during experiments and outcome assessment. Statistical tests were computed to test the correlation between datasets and/or the significance of specific features. The R programming language (v.3.1.2 and v.3.4.0)³⁸ was widely used for this purpose. In general, before applying any test, the normality of the distributions was tested by the Anderson–Darling normality test (R package nortest). The computation of tests such as the Wilcoxon rank-sum test (two-sided, unless otherwise specified) or Pearson and Spearman correlation coefficients were carried out using the core statistics functions in R. Pair-wise Pearson correlation coefficients were calculated across conditions on the averaged, binned OE data and visualized as heat maps with hierarchical clustering (Extended Data Fig. 4h).

Reporting summary. Further information on research design is available in the Nature Research Reporting Summary linked to this paper.

Data availability

The sequencing DamID data from this study are available from the Gene Expression Omnibus, accession number GSE112551.

Code availability

Custom code generated to perform the analysis in this study is available upon request.

23. Matoba, S. et al. Embryonic development following somatic cell nuclear transfer impeded by persisting histone methylation. *Cell* **159**, 884–895 (2014).
24. Houliston, E., Guilly, M. N., Courvalin, J. C. & Maro, B. Expression of nuclear lamins during mouse preimplantation development. *Development* **102**, 271–278 (1988).
25. Miyanari, Y. & Torres-Padilla, M. E. Control of ground-state pluripotency by allelic regulation of *Nanog*. *Nature* **483**, 470–473 (2012).
26. Servant, N. et al. HiC-Pro: an optimized and flexible pipeline for Hi-C data processing. *Genome Biol.* **16**, 259 (2015).
27. Vogel, M. J., Peric-Hupkes, D. & van Steensel, B. Detection of in vivo protein–DNA interactions using DamID in mammalian cells. *Nat. Protoc.* **2**, 1467–1478 (2007).
28. Martin, M. Cutadapt removes adapter sequences from high-throughput sequencing reads. *EMBnetjournal* **17**, 10–12 (2011).
29. Li, H. & Durbin, R. Fast and accurate short read alignment with Burrows–Wheeler transform. *Bioinformatics* **25**, 1754–1760 (2009).
30. Filion, G. J. et al. Systematic protein location mapping reveals five principal chromatin types in *Drosophila* cells. *Cell* **143**, 212–224 (2010).
31. Kim, D., Langmead, B. & Salzberg, S. L. HISAT: a fast spliced aligner with low memory requirements. *Nat. Methods* **12**, 357–360 (2015).
32. Anders, S., Pyl, P. T. & Huber, W. HTSeq—a Python framework to work with high-throughput sequencing data. *Bioinformatics* **31**, 166–169 (2015).
33. Robinson, M. D., McCarthy, D. J. & Smyth, G. K. edgeR: a Bioconductor package for differential expression analysis of digital gene expression data. *Bioinformatics* **26**, 139–140 (2010).
34. Park, S. J. et al. Inferring the choreography of parental genomes during fertilization from ultralarge-scale whole-transcriptome analysis. *Genes Dev.* **27**, 2736–2748 (2013).
35. Deng, Q., Ramsköld, D., Reinius, B. & Sandberg, R. Single-cell RNA-seq reveals dynamic, random monoallelic gene expression in mammalian cells. *Science* **343**, 193–196 (2014).
36. Bray, N. L., Pimentel, H., Melsted, P. & Pachter, L. Near-optimal probabilistic RNA-seq quantification. *Nat. Biotechnol.* **34**, 525–527 (2016).
37. Peric-Hupkes, D. et al. Molecular maps of the reorganization of genome–nuclear lamina interactions during differentiation. *Mol. Cell* **38**, 603–613 (2010).
38. R Core Team. *R: A Language and Environment for Statistical Computing* <http://www.R-project.org/> (R Foundation for Statistical Computing, Vienna, Austria, 2017).

Acknowledgements We thank members of the J.K. and M.-E.T.-P. laboratories and T. Straub (Biomedical Center, Ludwig-Maximilians-University) for helpful discussions and comments on the manuscript; I. Solovei, A. Scialdone and A. van Oudenaarden for critical reading of the manuscript; J. Gribnau (Erasmus UMC Rotterdam) for providing the embryonic stem cells and J. W. Jachowicz for embryo drawings. We thank R. Tepperino (Helmholtz Centre Munich) for support. We acknowledge funding by ERC-Stg EpiID (678423) to J.K. and EpiGeneSys NoE, ERC-Stg NuclearPotency (280840), the German Research Council (CRC 1064) and the Helmholtz Association to M.-E.T.-P. M.B. held a Boehringer Ingelheim Fonds PhD fellowship. The Oncode Institute is supported by KWF Dutch Cancer Society.

Author contributions M.B. performed the embryo work, S.M.P. managed the sequencing data and performed all bioinformatic analysis, except for the Hi-C data, which were analysed by M.B. and T.S. and the expression analysis in Extended Data Figs. 1h, 2f, h by E.R.R.-M. J.P. constructed the pipeline for 3D imaging analyses. K.L.d.L. optimized the single-cell DamID protocol. S.S.d.V. designed and performed experiments with the mouse embryonic stem cell DamID lines. M.B. and S.M.P. contributed to experimental design and data interpretation. M.-E.T.-P. and J.K. conceived, designed and supervised the project.

Competing interests The authors declare no competing interests.

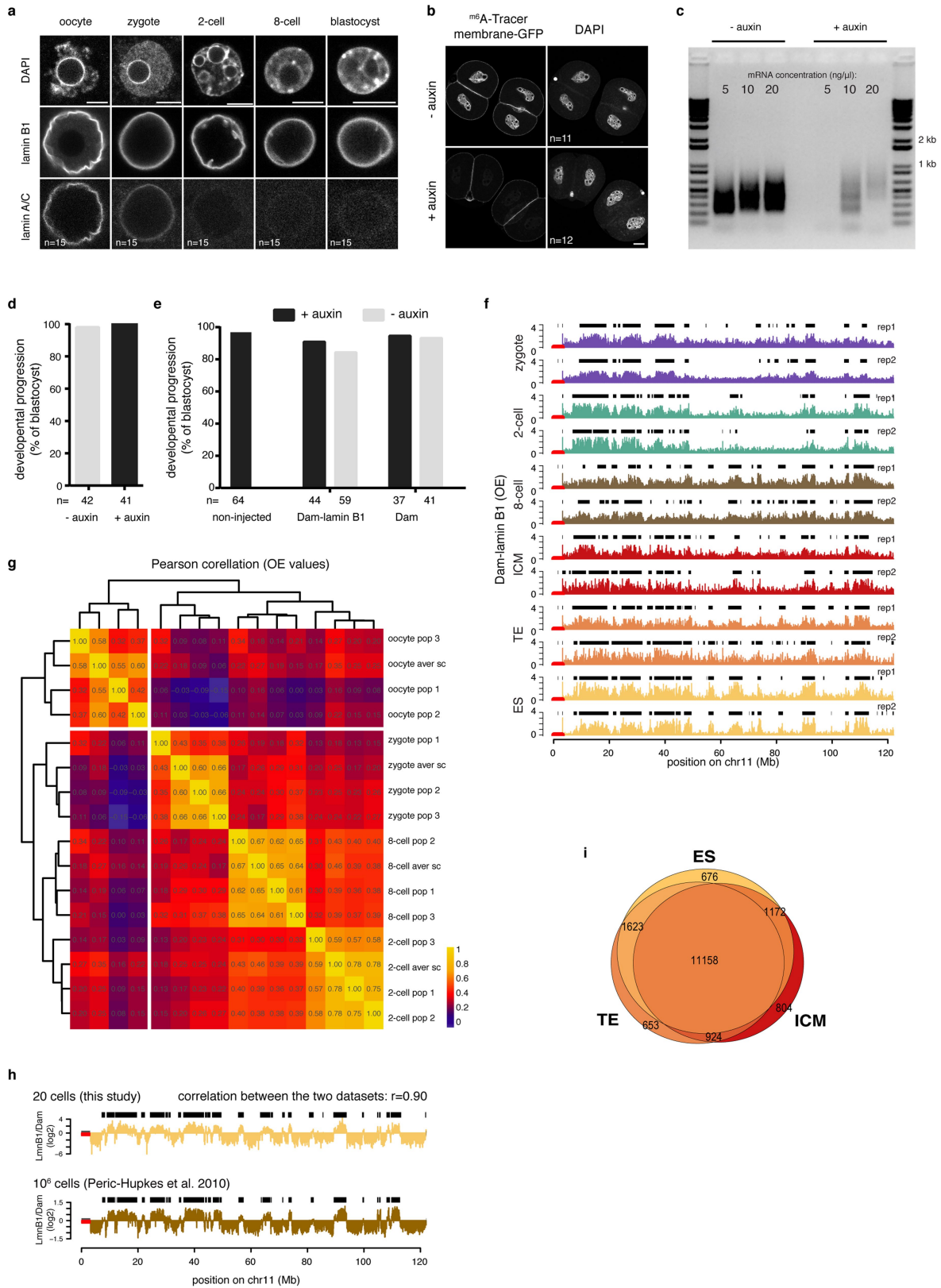
Additional information

Supplementary information is available for this paper at <https://doi.org/10.1038/s41586-019-1233-0>.

Correspondence and requests for materials should be addressed to M.-E.T.-P. or J.K.

Peer review information *Nature* thanks Katsuhiko Shirahige and the other anonymous reviewer(s) for their contribution to the peer review of this work.

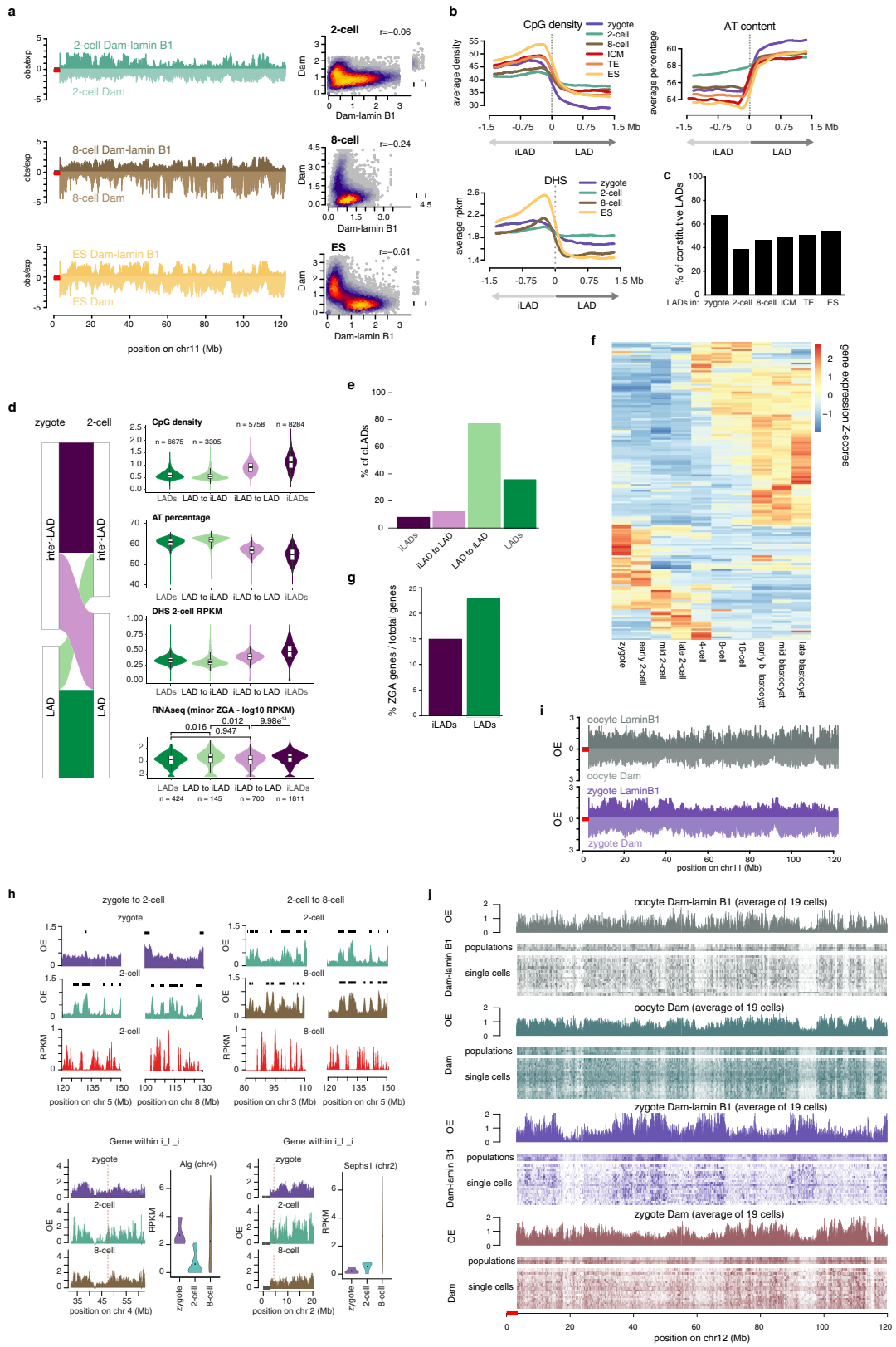
Reprints and permissions information is available at <http://www.nature.com/reprints>.



Extended Data Fig. 1 | See next page for caption.

Extended Data Fig. 1 | Establishment of DamID in mouse pre-implantation embryos. **a**, Immunostaining of lamin A/C and lamin B1 in oocytes, zygotes, 2-cell and 8-cell embryos and blastocysts. Scale bars, 5 μm . Levels were previously quantified by western blot in ref. ²⁴. Experiments were repeated at least three times. **b**, ^{m6}ATracer signals with and without auxin. Scale bar, 20 μm . Experiments were repeated at least three times with similar results. **c**, PCR smears amplified from ten 2-cell embryos injected with varying amounts of mRNA encoding Dam-lamin B1 and developed in the presence or absence of auxin. Experiments were repeated at least three times with similar results. **d**, Development to the blastocyst in the absence or presence of auxin. **e**, Development to the

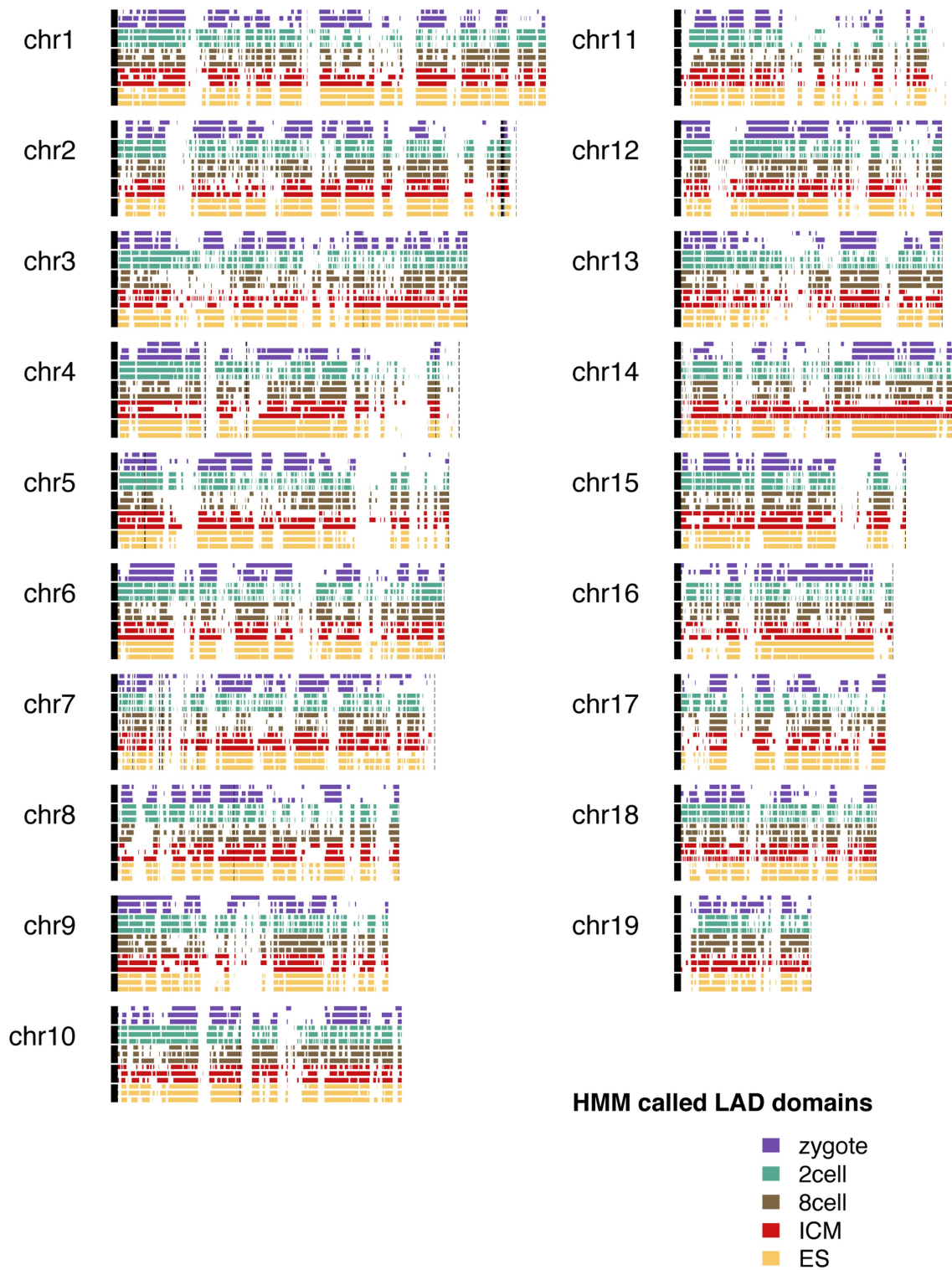
blastocyst of zygotes injected with Dam or Dam-lamin B1 mRNA in the absence or presence of auxin. **f**, Dam-lamin B1 profiles on chromosome 11. Black boxes represent LAD domains. **g**, Hierarchical clustering of Dam-lamin B1 population ($n = 3$) and average single cell profiles in oocyte ($n = 56$), zygote ($n = 19$), 2-cell ($n = 47$) and 8-cell stage ($n = 42$). $n =$ number of biologically independent samples. **h**, Comparison of genomic profiles obtained by DamID sequencing (this study) to previous DamID on micro-arrays. Black boxes represent LAD domains called by HMM. $r =$ Spearman's rho. **i**, Venn diagram showing overlap between LADs in embryonic stem cells, ICM and trophectoderm (TE).



Extended Data Fig. 2 | See next page for caption.

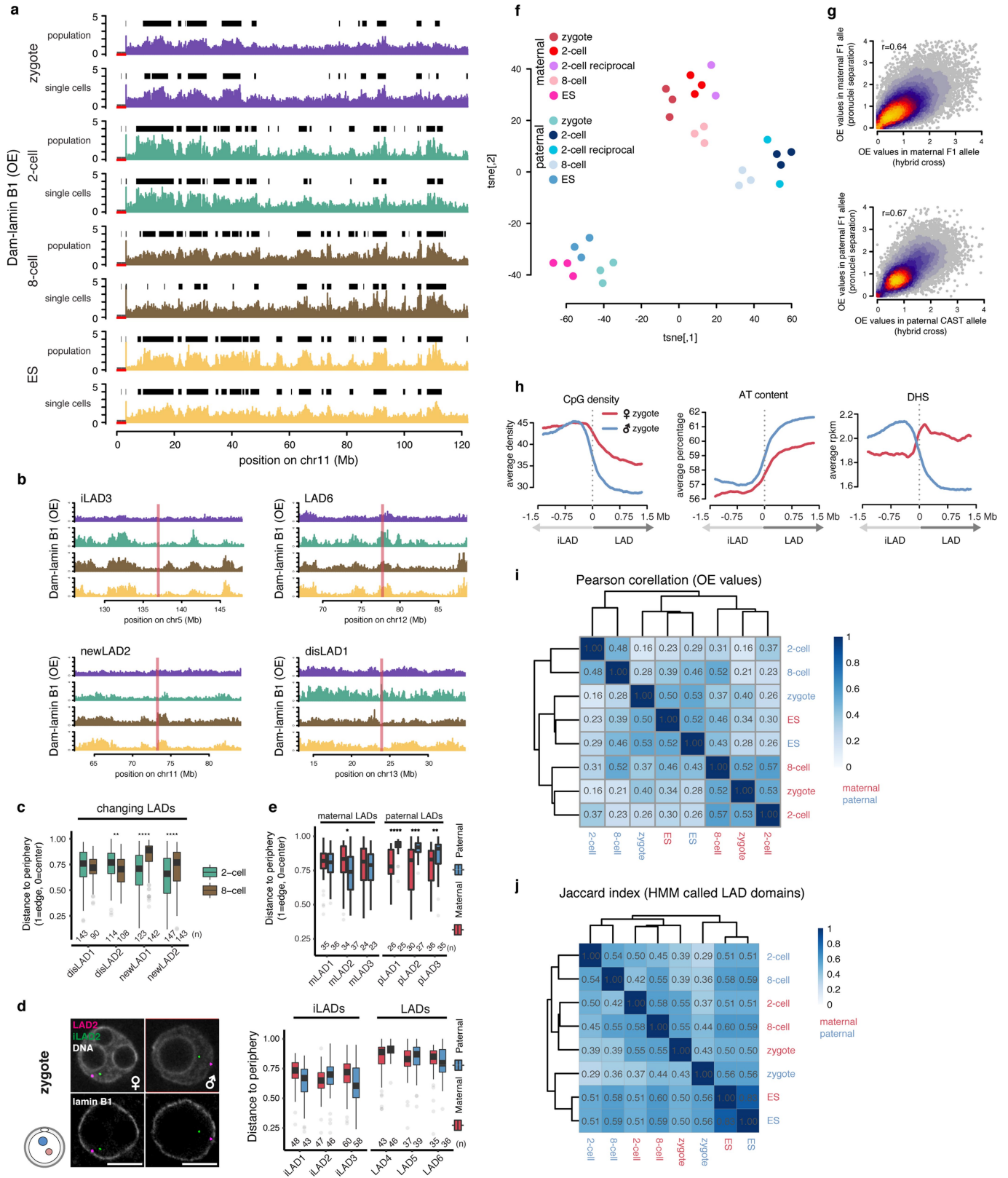
Extended Data Fig. 2 | Features of embryonic LADs, analysis of gene expression and oocyte DamID. **a**, Left, chromosome plots comparing Dam and Dam-lamin B1 DamID profiles in 2-cell embryos, 8-cell embryos and embryonic stem cells. Right, genome-wide comparison scatter plots of Dam and Dam-lamin B1 scores per 100-kb bin in 2- and 8-cell embryos and embryonic stem cells (right panel). DamID scores were calculated based on $n = 3$ independent biological replicates. $r =$ Spearman's rho. **b**, Average CpG density, AT content and DNaseI hypersensitivity sites (DHS)¹⁰ over LAD boundaries. **c**, Percentage overlap of LADs in embryos with constitutive LADs (associating with the lamina in embryonic stem cells, astrocytes, neural precursor cells and mouse embryonic fibroblasts)^{8,37}. **d**, CpG density, A/T content, DNaseI hypersensitivity (DHS) and minor ZGA gene expression at the 2-cell stage in genomic regions reorganizing in respect to the nuclear periphery during the zygote to 2-cell stage transition. Violin plots show the 25th and 75th percentiles (white boxes), median (black horizontal line) and values at most $1.5 \times$ IQR. For CpG density, A/T content and DHS, $n =$ number of bins; for minor ZGA expression, $n =$ number of minor ZGA genes. Wilcoxon rank-sum test P values shown (two-sided). DHS data from ref.¹³, expression data from ref.¹⁹. **e**, Percentage overlap of the de novo

iLAD at the 2-cell stage with constitutive LADs (as defined for c). **f**, Heat map of gene expression Z-scores at different stages of early embryonic development, depicting only genes in LADs specific to the 2-cell stage. These genomic regions contain 957 genes of which the 155 expressed genes are presented in the heat map (see Methods). **g**, Percentage of minor ZGA genes of total number of genes in iLADs (purple) and LADs (green). **h**, Example regions of LAD dynamics between the zygote and 2-cell stage (left top) and the 2-cell and 8-cell stage (right top). For each region, the mRNA expression levels are depicted in RPKM (red). The bottom panels display two examples of LAD dynamics between the zygote, 2-cell and 8-cell stages. The location of two genes in the 2-cell-specific LADs is indicated with a dotted line and the expression levels (RPKM) of the corresponding genes is displayed as violin plots. Violin plots show median (black points) and values at most $1.5 \times$ IQR. $n =$ biologically independent samples; zygote ($n = 4$), 2-cell ($n = 10$) and 8-cell ($n = 28$). **i**, Chromosome plot comparing Dam and Dam-lamin B1 profiles in oocytes and zygotes. **j**, Chromosome plots comparing Dam and Dam-lamin B1 DamID population and single-cell profiles in oocytes and zygotes.



Extended Data Fig. 3 | Chromosome interaction profiles of Dam-lamin B1 triplicate samples. Dam-lamin B1 chromosomal interaction maps from three biological replicate DamID population samples for each

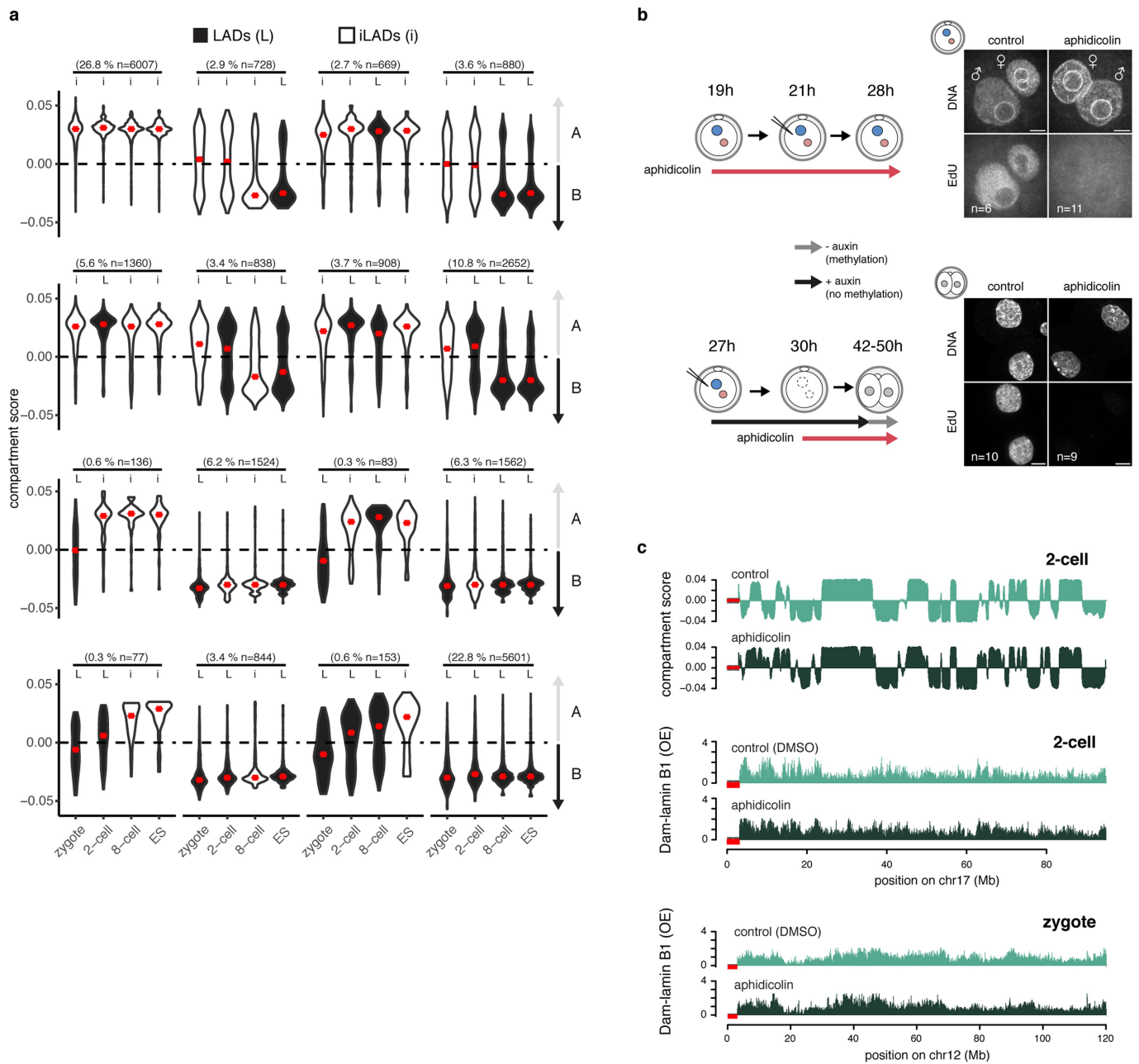
embryonic stage. Coloured blocks represent HMM-called LAD domains. Black bars on the left represent centromeres, red highlights indicate unmappable regions.

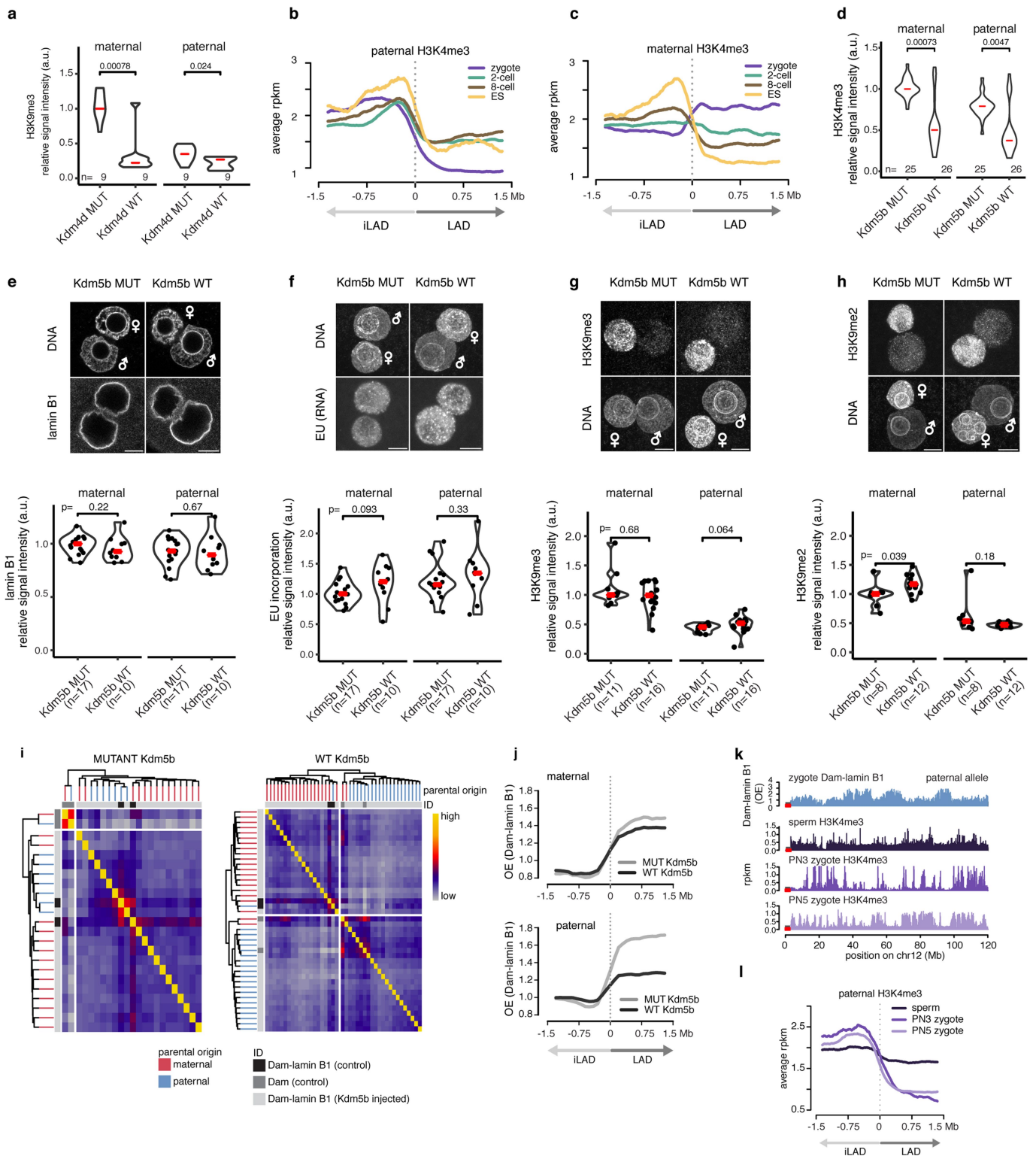


Extended Data Fig. 4 | See next page for caption.

Extended Data Fig. 4 | Single cells show consistent LAD patterning within the same developmental stages but parental genomes display distinct features. **a**, Chromosome profiles of population average ($n = 3$) and single-cell average Dam–lamin B1 signals. Black boxes represent LAD domains called by HMM. **b**, Genomic location of example DNA FISH probes projected on Dam–lamin B1 chromosome profiles. **c**, Quantification of 3D preserved DNA FISH spot distances to the nuclear periphery in 2-cell and 8-cell embryos of probes in regions that change LAD status between 2-cell and 8-cell stages according to DamID. Box plots show the 25th and 75th percentiles (box), median (solid lines), the smallest and largest values within $1.5 \times$ IQR of the hinge (whiskers) and outliers (grey circles). $n =$ number of DNA FISH spots from at least three biologically independent samples. Wilcoxon rank-sum test P values shown (two-sided). $**P \leq 0.01$, $****P \leq 0.0001$. **d**, Images of 3D DNA FISH in zygote pronuclei. Quantification shows distance to the nuclear periphery. Scale bars, $10 \mu\text{m}$. Box plots show the 25th and 75th percentiles (box), median (solid lines), the smallest and largest values within $1.5 \times$ IQR of the hinge (whiskers) and outliers (grey circles). $n =$ number of DNA FISH

spots from at least three biologically independent samples. **e**, Distance quantification of DNA FISH probes in maternal and paternal specific LADs in zygotes. Box plots show the 25th and 75th percentiles (box), median (solid lines), the smallest and largest values within $1.5 \times$ IQR of the hinge (whiskers) and outliers (grey circles). $n =$ number of DNA FISH spots from at least three biologically independent samples. Wilcoxon rank-sum test P values shown (two-sided). $*P \leq 0.05$, $**P \leq 0.01$, $***P \leq 0.001$, $****P \leq 0.0001$. **f**, t -SNE representation of the triplicate allelic Dam–lamin B1 population samples, including 2-cell embryos from reciprocal crosses. $n = 3$ biologically independent samples. **g**, Scatter plot comparison between average Dam–lamin B1 signals obtained from pronucleus separated and hybrid zygote DamID. $n =$ biologically independent samples. Maternal pronucleus ($n = 10$), paternal pronucleus ($n = 15$) and hybrid zygote ($n = 3$). $r =$ Spearman's rho. **h**, Average CpG density, AT content and DHS sites over LAD boundaries ± 1.5 Mb defined specifically for maternal and paternal alleles in zygotes. **i**, Allelic correlation matrix (Pearson) of OE scores from Dam–lamin B1 embryos. **j**, Jaccard indexes calculated over HMM-called LAD domains.





Extended Data Fig. 6 | See next page for caption.

Extended Data Fig. 6 | Overexpression of *Kdm5b* histone demethylase abrogates paternal LAD establishment in the zygote. **a**, Quantifications of immunostaining with H3K9me3 in zygotes injected with wild-type and mutant KDM4D. Violin plots show the values at most $1.5 \times$ IQR and median (red lines). $n =$ at least three biologically independent samples. Wilcoxon rank-sum test P values shown (two-sided).

b, Average paternal-specific H3K4me3 signal at paternal-specific LAD boundaries of each respective embryonic stage. **c**, Average maternal specific H3K4me3 signal at maternal specific LAD boundaries of each respective embryonic stage. **d**, Quantification as described for **a** but with H3K4me3. **e**, Immunostaining and quantification of lamin B1 localization in the *Kdm5b*-expressing zygotes. **f**, Global transcription detection (EU incorporation) and quantification in H3K4me3 in the *Kdm5b*-expressing zygotes. **g**, Immunofluorescent staining of H3K9me3 in mutant and wild-

type KDM5B-expressing embryos. **h**, Immunofluorescent staining of H3K9me2 in mutant and wild-type KDM5B injected embryos.

i, Hierarchical clustering based on Pearson correlation of Dam–lamin B1 signal from single pronuclei of wild-type and mutant *Kdm5b*-injected zygotes (samples from three independent experiments). For comparison, population average Dam and Dam–lamin B1 signals are included as grey and black squares, respectively. **j**, Average Dam–lamin B1 signal at LAD boundaries in hybrid H3K4me3 manipulated embryos. Signal shown in maternal genome (top) and paternal genome (bottom). **k**, Chromosome profiles of H3K4me3 ChIP with sequencing (ChIP-seq)²⁰ signal from sperm, early zygotes and late zygotes. **l**, Average H3K4me3 levels in sperm, early zygotes and late zygotes at paternal zygotic LAD borders. In **e–h**, violin plots show the values at most $1.5 \times$ IQR and median (red lines); Wilcoxon rank-sum test P values shown (two-sided). Scale bars, 10 μ m.

Reporting Summary

Nature Research wishes to improve the reproducibility of the work that we publish. This form provides structure for consistency and transparency in reporting. For further information on Nature Research policies, see [Authors & Referees](#) and the [Editorial Policy Checklist](#).

Statistical parameters

When statistical analyses are reported, confirm that the following items are present in the relevant location (e.g. figure legend, table legend, main text, or Methods section).

n/a | Confirmed

- The exact sample size (n) for each experimental group/condition, given as a discrete number and unit of measurement
- An indication of whether measurements were taken from distinct samples or whether the same sample was measured repeatedly
- The statistical test(s) used AND whether they are one- or two-sided
Only common tests should be described solely by name; describe more complex techniques in the Methods section.
- A description of all covariates tested
- A description of any assumptions or corrections, such as tests of normality and adjustment for multiple comparisons
- A full description of the statistics including central tendency (e.g. means) or other basic estimates (e.g. regression coefficient) AND variation (e.g. standard deviation) or associated estimates of uncertainty (e.g. confidence intervals)
- For null hypothesis testing, the test statistic (e.g. F , t , r) with confidence intervals, effect sizes, degrees of freedom and P value noted
Give P values as exact values whenever suitable.
- For Bayesian analysis, information on the choice of priors and Markov chain Monte Carlo settings
- For hierarchical and complex designs, identification of the appropriate level for tests and full reporting of outcomes
- Estimates of effect sizes (e.g. Cohen's d , Pearson's r), indicating how they were calculated
- Clearly defined error bars
State explicitly what error bars represent (e.g. SD, SE, CI)

Our web collection on [statistics for biologists](#) may be useful.

Software and code

Policy information about [availability of computer code](#)

Data collection

No software was used for data collection.

Data analysis

DNA-FISH images were analyzed with Icy - Version 1.9.5.1 (<http://icy.bioimageanalysis.org>) with a custom made protocol available upon request. HiC data was analyzed with HiC-Pro (version 2.10.0) (doi:10.1186/s13059-015-0831-x). Compartments were called using the HiTC Bioconductor package Release (3.6) (10.1093/bioinformatics/bts521). Cutadapt (<http://dx.doi.org/10.14806/ej.17.1.200>) was used to trim the fastq reads; pre-processed reads were aligned to the reference genome using bwa (version bwa-0.7.12) (DOI: 10.1093/bioinformatics/btp324) ; SNPsplit_genome_preparation (version SNPsplit_v0.3.0/) (<http://www.bioinformatics.babraham.ac.uk/projects/SNPsplit/>) was used for the nucleotide substitution in the mm10 genome assembly; PCR duplicates were removed using picard tools (version picard-tools-1.130) (<http://broadinstitute.github.io/picard/>); hisat2 (version hisat2-2.0.3-beta) (DOI: 10.1038/nmeth.3317) was used to align mRNA reads to a the mm10 transcriptional model and htseq-count (version 0.6.0) (doi: 10.1101/002824) and kallisto (version 0.44.0) (doi: 10.1038/nbt.3519) were used to quantify the counts; the R programming language (versions R-3.1.2, R-3.4.0 and R-3.4.3) (<https://www.R-project.org/>) was widely used within the study for statistical analysis and data plotting. The R package edgeR (doi: 10.1093/bioinformatics/btp616) was used for RNA expression differential analysis. Pheatmap was used for the generation of heatmaps of relative gene expression (version 1.10.12) (<https://cran.r-project.org/web/packages/pheatmap/>). Basecalling and filtering were performed using standard software of the Illumina HiSeq 2500 (<https://www.illumina.com/systems/sequencing-platforms/hiseq-2500.html>).

For manuscripts utilizing custom algorithms or software that are central to the research but not yet described in published literature, software must be made available to editors/reviewers upon request. We strongly encourage code deposition in a community repository (e.g. GitHub). See the Nature Research [guidelines for submitting code & software](#) for further information.

Data

Policy information about [availability of data](#)

All manuscripts must include a [data availability statement](#). This statement should provide the following information, where applicable:

- Accession codes, unique identifiers, or web links for publicly available datasets
- A list of figures that have associated raw data
- A description of any restrictions on data availability

Data produced in this study is available at GSE112551. Publicly available data used for RNAseq and H3K4me3 ChIPseq can be found under the accession numbers GSE45719 and GSE71434; for HiC data at GSE82185 and PRJCA000241.

Figures with associated raw data: figure 1b, figure 1c, figure 1d, figure 1e, figure 1h, figure 1j, figure 2a, figure 2b, figure 2d, figure 2e, figure 2f, figure 2g, figure 3b, figure 3d, figure 3h, figure 4c, figure 4f, figure 4g, figure s1f, figure s1g, figure s1h, figure s2a, figure s2h, figure s2i, figure s3, figure s4a, figure s4b, figure s4f, figure s4g, figure s4j, figure s4j, figure s5c, figure s6h, figure s6g, figure s6i.

Field-specific reporting

Please select the best fit for your research. If you are not sure, read the appropriate sections before making your selection.

Life sciences Behavioural & social sciences Ecological, evolutionary & environmental sciences

For a reference copy of the document with all sections, see [nature.com/authors/policies/ReportingSummary-flat.pdf](https://www.nature.com/authors/policies/ReportingSummary-flat.pdf)

Life sciences study design

All studies must disclose on these points even when the disclosure is negative.

Sample size	Three biological replicates were generated for all stages. These biological replicates showed high concordance and increasing sample size beyond three would not result in increased data quality improvement (reduce false positives/negatives).
Data exclusions	Samples with less than 30,000 unique GATCs were excluded from the data.
Replication	Experiments were successfully replicated n=3 or more
Randomization	In each experiment embryos from 4-8 female mice were pooled and randomly allocated to experimental groups.
Blinding	No blinding was done, since no manual assessment of images or experimets was performed

Reporting for specific materials, systems and methods

Materials & experimental systems

n/a	Involvement	Involved in the study
<input type="checkbox"/>	<input checked="" type="checkbox"/>	Unique biological materials
<input type="checkbox"/>	<input checked="" type="checkbox"/>	Antibodies
<input type="checkbox"/>	<input checked="" type="checkbox"/>	Eukaryotic cell lines
<input checked="" type="checkbox"/>	<input type="checkbox"/>	Palaeontology
<input type="checkbox"/>	<input checked="" type="checkbox"/>	Animals and other organisms
<input checked="" type="checkbox"/>	<input type="checkbox"/>	Human research participants

Methods

n/a	Involvement	Involved in the study
<input checked="" type="checkbox"/>	<input type="checkbox"/>	ChIP-seq
<input checked="" type="checkbox"/>	<input type="checkbox"/>	Flow cytometry
<input checked="" type="checkbox"/>	<input type="checkbox"/>	MRI-based neuroimaging

Unique biological materials

Policy information about [availability of materials](#)Obtaining unique materials

Antibodies

Antibodies used

Lamin B1 sc-6216 Santa Cruz (1:100)
 Lamin A/C 39288 Active Motif (1:200)
 mAb414 (nuclear pores) ab24609 Abcam (1:1000)
 HA-tag 11867423001 Roche (1:250)
 H3K4me3 C15410003 Diagenode (1:250)
 H3K9me2 07-441 Millipore Upstate (1:250)
 H3K9me3 17-625 Millipore Upstate (1:250)
 488 GAR Life Tech A11034 (1:500)
 488 GAM Invitrogen A11001 (1:500)
 647 GAR Life Tech A21245 (1:500)
 647 GAM Life Tech A21236 (1:500)

Validation

Lamin B1 antibody was validated in KO mESC (DOI: 10.1126/science.1211222). mAb414 antibody was validated in preimplantation embryo (doi:10.1038/nsmb.2839). HA-tag antibody is validated by the manufacturer (<https://www.sigmaaldrich.com/catalog/product/roche/roahaha?lang=de®ion=DE>). H3K4me3 antibody is validated on dot-blot by the manufacturer (<https://www.diagenode.com/en/p/h3k4me3-polyclonal-antibody-premium-50-ug-50-ul>). Lamin A/C antibody is validated on KO mESC (doi:10.4161/nucl.23384). H3K9me2 antibody was validated by the manufacturer (http://www.merckmillipore.com/HU/hu/product/Anti-dimethyl-Histone-H3-Lys9-Antibody,MM_NF-07-441?ReferrerURL=https%3A%2F%2Fwww.google.hu%2F). H3K9me3 antibody was validated by the manufacturer (http://www.merckmillipore.com/HU/hu/product/ChIPAb+-Trimethyl-Histone-H3-Lys9-ChIP-Validated-Antibody-and-Primer-Set,MM_NF-17-625?ReferrerURL=https%3A%2F%2Fwww.google.hu%2F).

Eukaryotic cell lines

Policy information about [cell lines](#)

Cell line source(s)

Authentication

Mycoplasma contamination

Commonly misidentified lines
(See [ICLAC](#) register)

Animals and other organisms

Policy information about [studies involving animals](#); [ARRIVE guidelines](#) recommended for reporting animal research

Laboratory animals

Wild animals

Field-collected samples